J. Membrane Biol. 179, 243–262 (2001)
DOI: 10.1007/s002320010050

The Journal of
Membrane
Biology

Ni^{2+} Slows the Activation Kinetics of High-Voltage-Activated Ca^{2+} Currents in Cortical Neurons: Evidence for a Mechanism of Action Independent of Channel-Pore Block

J. Magistretti*, S. Brevi, M. de Curtis

Laboratorio di Biofisica e Neurofisiologia dei Sistemi Corticali, Dipartimento di Neurofisiologia Sperimentale, Istituto Nazionale Neurologico "Carlo Besta", Via Celoria 11, 20133 Milano, Italy

Received: 13 July 2000/Revised: 9 November 2000

Abstract. The effects of Ni^{2+} were evaluated on slowly-decaying, high-voltage-activated (HVA) Ca^{2+} currents expressed by pyramidal neurons acutely dissociated from guinea-pig piriform cortex. Whole-cell, patch-clamp recordings were performed with Ba^{2+} as the charge carrier. Ni^{2+} blocked HVA Ba^{2+} currents (I_{Ba}s) with an EC_{50} of approximately 60 μM. Additionally, after application of nonsaturating Ni^{2+} concentrations, residual currents activated with substantially slower kinetics than both total and Ni^{2+}-sensitive I_{Ba}s. None of the pharmacological components of slowly decaying, HVA currents activated with kinetics significantly different from that of total currents, indicating that the effect of Ni^{2+} on I_{Ba}s kinetics cannot be attributed to the preferential inhibition of a fast-activating component. The effect of Ni^{2+} on I_{Ba} amplitude was voltage-independent over the potential range normally explored in our experiments (−60 to +20 mV), hence the Ni^{2+}-dependent decrease of I_{Ba} activation rate is not due to a voltage- and time-dependent relief from block. Moreover, Ni^{2+} significantly reduced I_{Ba} deactivation speed upon repolarization, which also is not compatible with a depolarization-dependent unblocking mechanism. The dependence on Ni^{2+} concentration of the I_{Ba} activation-rate reduction was remarkably different from that found for I_{Ba} block, with an EC_{50} of ~20 μM and a Hill coefficient of ~1.73 *vs.* ~1.10. These results demonstrate that Ni^{2+}, besides inhibiting the I_{Ba}s under study probably by exerting a blocking action on the pore of the underlying Ca^{2+} channels, also interferes with Ca^{2+}-channel gating kinetics, and strongly suggest that the two effects depend on Ni^{2+} occupancy of binding sites at least partly distinct.

Key words: Calcium currents — Nickel — Block — Activation kinetics — Channel gating — Patch clamp

Introduction

Several divalent cations of groups VII to IIB are known to exert a blocking effect on voltage-gated Ca^{2+} channels. Among them, cadmium (Cd^{2+}) and nickel (Ni^{2+}) ions represent the two most extensively studied examples. The effects of these cations on voltage-gated Ca^{2+} conductances have been characterized both at the whole-cell and single-channel level. Their mechanism of action has been recognized to consist in the interaction with a binding site located within the channel pore (Lansman, Hess & Tsien, 1986; Swandulla & Armstrong, 1989; Winegar, Kelly & Lansman, 1991; Chow, 1991; Yang et al., 1993), leading to high-affinity occupancy and occlusion of the permeation path. In particular, Ni^{2+} has been shown to behave as a channel-pore blocker acting in a "fast" time scale (*see* Hille, 1992), thus causing, at the single-channel level, a very rapid "flickering" of openings (Chesnoy-Marchais, 1985) or an apparent decrease of unitary-current amplitude (Winegar et al., 1991).

The blocking effect exerted by Ni^{2+} takes place with different potencies depending on the specific Ca^{2+}-current or -channel type considered. Historically, Ni^{2+} has been considered a relatively specific agent for low-voltage-activated (LVA), T-type Ca^{2+} currents, since early studies on dorsal-root-ganglion neurons revealed a higher potency of Ni^{2+} block for LVA currents than for high-voltage-activated (HVA) currents (Fox, Nowycky

* *Permanent address:* Dipartimento di Scienze Fisiologiche-Farmacologiche-Cellulari-Molecolari, Sezione di Fisiologia Generale e Biofisica Cellulare, Università degli Studi di Pavia, Via Forlanini 6, 27100, Pavia, Italy.

Correspondence to: J. Magistretti

& Tsien, 1987; Carbone & Swandulla, 1989). Later on, such results have been confirmed for some neuronal populations of the central nervous system (CNS) (Crunelli, Lightowler & Pollard, 1989; Ozawa et al., 1989; Allen, Sim & Brown, 1993; Lucaj & Fujii, 1994), whereas in several other CNS structures, including spinal cord (Huang, 1989), amygdala (Kaneda & Akaike, 1989), hippocampus (Takahashi & Akaike, 1991; Fraser & MacVicar, 1991), piriform cortex (S. Brevi, M. de Curtis and J. Magistretti, *in preparation*), and neocortex (Ye & Akaike, 1993), Ni^{2+} turned out to be a much less potent blocker of T-type currents (*see also* Carbone & Swandulla, 1989). These discrepancies can now be explained on the basis of the currently available data on the molecular determinants of T-type channels. Three different α_1 subunits accounting for T-type channels (α_{1G}, α_{1H}, α_{1I}) have been isolated so far (Perez-Reyes, 1998; Lee et al., 1999*a*), on each of which Ni^{2+} displays a different blocking potency (Lee et al., 1999*b*), with the highest potency for α_{1H}, and the lowest for α_{1G}. Since the expression of each one of these subunits can be remarkably specific in different neuronal populations and at different developmental stages, the variable sensitivity to Ni^{2+} showed by functionally homogeneous T-type currents in native neurons can now be attributed to molecular differences of the underlying major channel subunits.

More recently, Ni^{2+} has also been found to be a more potent blocker of Ca^{2+} channels resulting from the expression of α_{1E}-type subunits than other HVA channels (Soong et al., 1993; Ellinor et al., 1993; Zhang et al., 1993; Williams et al., 1994; Schneider et al., 1994; Wakamori et al., 1994). α_{1E}-type subunits are believed, or have been demonstrated, to be responsible for the expression of a specific pharmacological fraction of HVA currents of native neurons, namely R-type currents, most of which also display high sensitivity to Ni^{2+} (*see also* Tottene, Volsen & Pietrobon, 2000). Ni^{2+} has thus been given considerable importance as a pharmacological tool for isolating specific Ca^{2+}-current subtypes, and has been widely used not only in biophysical characterizations of Ca^{2+} currents and channels but also in functional studies of neuronal Ca^{2+}-dependent events (e.g., Gillessen & Alzheimer, 1997; Sabatier, Richard & Dayanithi, 1997; Wang, Rowan & Anwyl, 1997; Bao, Li & Perl, 1998; Beurrier et al., 1999; Magee & Carruth, 1999).

In addition to the usual blocking effect, a limited number of studies have reported Ni^{2+}-dependent modifications of Ca^{2+}-current gating properties. A slowing of activation kinetics has been observed to be caused by Ni^{2+} on T-type currents of cultured rat hypothalamic neurons, and has been suggested to be the consequence of a voltage- and time-dependent mechanism of relief from block (Müller, Misgeld & Swandulla, 1992). Millimolar concentrations of Ni^{2+} have been shown to decrease the activation speed of P-type HVA currents in squid giant fiber lobe neurons, but in that case a Ni^{2+}-dependent stabilization of closed channel state(s) was rather implicated (McFarlane & Gilly, 1998). No data are available so far as to the possible existence of similar effects of Ni^{2+} on the kinetic properties of Ca^{2+} currents in native vertebrate neurons. Given the above-reminded importance of Ni^{2+} as a pharmacological tool for the dissection of functionally distinct Ca^{2+}-current fractions, such an issue can be of considerable experimental importance.

In previous experimental studies we characterized the biophysical and pharmacological properties of voltage-gated Ca^{2+} currents expressed by pyramidal neurons acutely dissociated from guinea-pig piriform-cortex layer II (Magistretti, Brevi & de Curtis, 1999, 2000). We also looked for the possible existence of differences in Ni^{2+} sensitivity of different current components. Here we show that, besides exerting a blocking effect, Ni^{2+} significantly decreases the activation speed of slowly decaying HVA currents in the same neurons. We demonstrate that this effect is not due to a mechanism of voltage- and time-dependent relief from block, and conclude that Ni^{2+} directly interferes with the kinetics of Ca^{2+}-channel state transitions. We also discuss some of the possible artifactual consequences that this action of Ni^{2+} may have on the study of the biophysical properties of voltage-gated Ca^{2+} currents.

Materials and Methods

Cell Preparation

The procedure followed for isolating piriform-cortex layer-II pyramidal neurons has been described elsewhere (Magistretti & de Curtis, 1998; Magistretti et al., 1999). Briefly, female Hartley guinea pigs (8–40 days old) were anaesthetized with an intraperitoneal injection of ketamine (200–250 mg/kg). After decapitation, the brain was quickly extracted under hypothermic conditions, the two hemispheres were separated, and each was cut with a McIlwain tissue chopper (Mickle, Gomshall, UK) into 500 μm-thick quasi-coronal slices, whose plane was normal to the main axis of the lateral olfactory tract. Layer II of anterior piriform cortex was carefully dissected from each slice under microscopic control. Cells were isolated from the layer-II tissue fragments thus obtained by means of an enzymatic (using 1 mg/ml protease type XIV, Sigma, St. Louis, MO) and mechanical dissociation procedure. The experimental procedure was approved by the Ethical Committee of the Istituto Nazionale Neurologico "C. Besta" in accordance with international regulations on animal research.

Patch-Clamp Recordings

The recording chamber was mounted on the stage of an Axiovert 100 microscope (Zeiss, Oberkochen, FRG). The cells were observed at ×400 magnification. After cell seeding, the chamber was perfused with an oxygenated extracellular solution suitable for isolating Ba^{2+} currents conducted through Ca^{2+} channels, containing (in mmol/l): 88 choline-

Cl, 40 tetraethylammonium (TEA)-Cl, 3 KCl, 2 $MgCl_2$, 5 $BaCl_2$, 3 CsCl, 10 N-[2-hydroxyethyl]piperazine-N′-[2-ethanesulfonic acid] (HEPES), 5, 4-aminopyridine, and 25 D-glucose (pH 7.4 with HCl). Perfusion rate was about 0.5 ml/min. Patch pipettes were made from thick-wall borosilicate glass capillaries (GC 150–7.5; Clark Electromedical Instruments, Reading, UK) by means of a Narishige PP-830 vertical puller. The pipette solution contained (in mmol/l): 78 Cs methanesulfonate (obtained by neutralizing CsOH with equimolar methanesulphonic acid), 40 TEA-Cl, 10 HEPES, 10 ethylene glycol-*bis*(β-aminoethyl ether) N,N,N′,N′-tetraacetic acid (EGTA), 20 phosphocreatine di-Tris salt, 2 adenosine 5′-triphosphate-Mg, 1 adenosine 3′,5′ cyclic monophosphate, and 20 U/ml creatinephosphokinase (pH adjusted to 7.2 with TEA-OH). The patch pipettes had a resistance of 4–6 MΩ when filled with the above solution. Tight seals (>10 GΩ) and the whole-cell configuration were obtained according to the standard technique (Hamill et al., 1981). Voltage-clamp recordings of Ba^{2+} currents were performed at room temperature (22°C) by means of an Axopatch 1D amplifier (Axon Instruments, Foster City, CA). After the establishment of the whole-cell condition, Ba^{2+} currents were allowed to stabilize for a few minutes before starting data acquisition. Series resistance (R_s) was evaluated on line by canceling the whole-cell capacitive transients evoked by −10-mV voltage square pulses with the amplifier's compensation section, and reading out the corresponding value. R_s was always compensated by 75–95%, and continually monitored during the experiment. The *lag* potentiometer of the amplifier's R_s compensation section was set to the lowest value compatible with ringing avoidance, normally 20–40 μsec. Recordings in which R_s levels varied with time by more than 2 MΩ were discarded. Voltage protocols were commanded and current signals were acquired with a Pentium personal computer interfaced to an Axon DigiData 1200 interface, using the Clampex program of the pClamp 6.0.3 software package (Axon Instruments). In all recordings the general holding potential was −70 mV. Every test voltage protocol was preceded by a 2-sec conditioning prepulse at −60 or −50 mV. Current signals were filtered at 5 kHz, digitized at 20 (ramp protocols and 300-msec step protocols) or 50 (deactivation protocols and other short step protocols) kHz, and online leak subtracted *via* a P/4 protocol.

Drug Application

$NiCl_2$ (purity degree = 99.9999%; Sigma-Aldrich, Milano, Italy) and organic Ca^{2+}-channel blockers were applied through a local-perfusion system consisting of a multibarrel pipette (diameter at the tip ~150 μm) in which each single barrel was connected to a separate perfusion channel. Upon opening independently each channel by operating on remote-commanded pinch electrovalves (Sirai, Milano, Italy), the drug-containing solution flowed by gravity, thus forming a laminar-flux cone. The tip of the perfusion pipette was positioned in close proximity of the recording site, so that the recorded cell was fully drenched by the laminar-flux cone. Organic Ca^{2+}-channel blockers were dissolved, stored and administered as described elsewhere (Magistretti et al., 1999).

Data Analysis

Current traces were analyzed by means of the Clampfit program of pClamp 6.0.3. Currents were normally refiltered offline at 1–2 kHz, unless preservation of high-frequency signal components was required (namely when tail currents were analyzed). Ba^{2+} permeabilities (P_{Ba}s) were calculated from peak current amplitudes (I_{Ba}s) by applying the constant-field (Goldman) equation in the form:

$$P_{Ba} = I_{Ba} \cdot (RT/4F^2V) \cdot [1 - \exp(-2FV/RT)]/\{[Ba^{2+}]_i - [Ba^{2+}]_o \cdot \exp(-2FV/RT)\},$$

where V is the membrane potential, and the concentrations $[Ba^{2+}]_i$ and $[Ba^{2+}]_o$ were given their nominal values (0 and 5 mM, respectively). Data were fitted with exponential functions, $I_{Ba} = \sum A_i \cdot \exp(-t/\tau_i) + C$, using Clampfit, and with Boltzmann functions, $P_{Ba} = P_{Ba(max)}/\{1 + \exp[(V - V_{1/2})/k]\}$, or other functions using Origin 6.0 (MicroCal Software, Northampton, MA). Average values were expressed as mean ± SEM. Statistical significance was evaluated by means of the Student's *t* test (two-tail test for unpaired data unless explicitly stated otherwise).

Computer Simulations

For a numerical reconstruction of ramp-activated I_{Ba}s, we applied the Goldman relationship:

$$I_{Ba}(V,t) = P_{Ba}(V,t) \cdot (4F^2V/RT) \cdot \{[Ba^{2+}]_i - [Ba^{2+}]_o \cdot \exp(-2FV/RT)\}/[1 - \exp(-2FV/RT)], \quad (1)$$

where

$$P_{Ba}(V,t) = P_{Ba(max)} \cdot m(V,t), \quad (2)$$

and

$$m(V,t) = m_\infty(V) - [m_\infty(V) - m_0] \cdot \exp[-t/\tau_{act}(V)]. \quad (3)$$

The function describing $m_\infty(V)$ was derived directly from the Boltzmann fitting of the average $P_{Ba}(V)$ plot (*see* Fig. 5*B*). The functions describing $\tau_{act}(V)$ both in control conditions and during Ni^{2+} application are described in the Results. The time course of ramp-evoked I_{Ba}s was numerically reconstructed on the basis of the Eqs. 1 and 2, and Eq. 3 in its differential form. The simulation programs were compiled using QuickBASIC 4.5 (Microsoft).

Results

Ni^{2+} Ions Reduce Both Amplitude and Activation Speed of HVA I_{Ba}s in Guinea-Pig Piriform-Cortex Neurons

Voltage-dependent Ba^{2+} currents (I_{Ba}s) were elicited by delivering step depolarizations starting from 2-sec prepulses at −60 mV, which allowed us to record HVA currents in isolation (*see* Magistretti & de Curtis, 1998). We have previously shown that, in the neuronal preparation under study, total I_{Ba}s consist of multiple pharmacological components (L-, N- and R-type components infrequently associated with a small P/Q-type component) and can display remarkably variable kinetic properties. To avoid uncertainties deriving from heterogeneity in I_{Ba} biophysical properties, the present study was strictly limited to slowly inactivating currents, in which the fractional decay after the 300 msec of the routinely applied voltage pulses was lower than 0.2 at the peak of the *I-V* relationship (usually occurring at 0 mV).

Figure 1*A1* and *B1* shows examples of such currents recorded with test pulses at 0 mV in two different neurons. The application of 50-μM Ni^{2+} reduced peak cur-

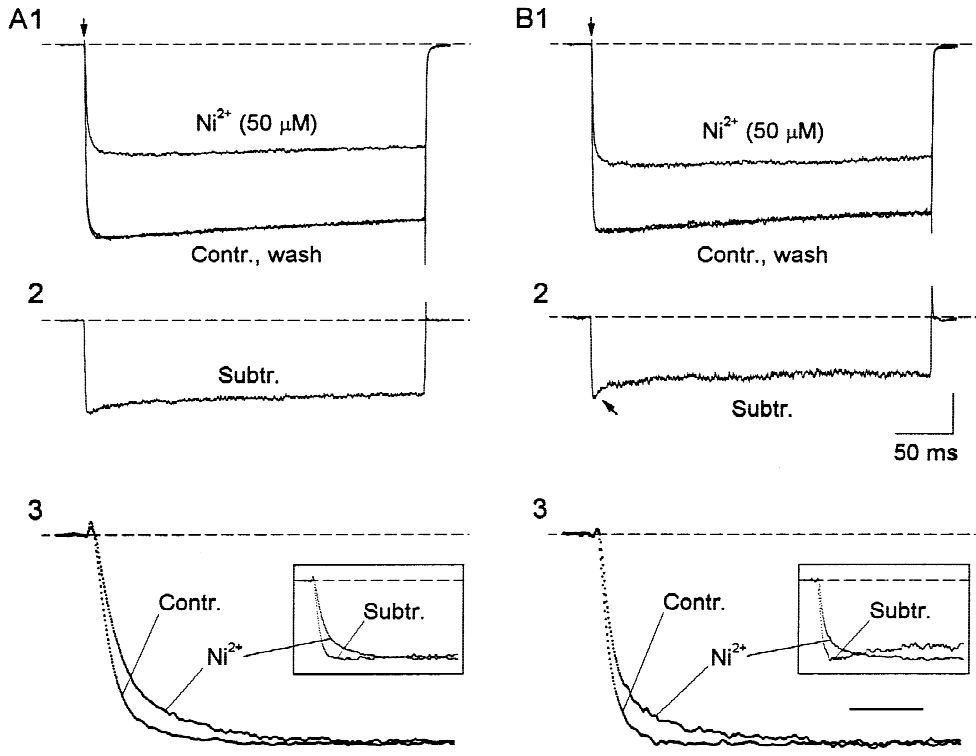

Fig. 1. Ni^{2+} reduces both amplitude and activation speed of HVA I_{Ba}s in guinea-pit piriform-cortex neurons. (*A*), (*B*) Effects of Ni^{2+} on HVA I_{Ba}s evoked with 300-msec voltage square pulses at 0 mV (starting at the time points marked by arrows in the two upper panels) in two representative neurons (cell A9304 in *A*, A9218 in *B*). Panels *A1* and *B1* show I_{Ba}s recorded before and during application of 50-μM Ni^{2+} and after washout of the cation, panels *A2* and *B2* show the current fractions blocked by Ni^{2+}, obtained by subtraction (*y*-axis scale: 600 pA in *A*, 200 pA in *B*). The arrow in *B2* points at the transient, fast-decaying component frequently observed at the beginning of Ni^{2+}-sensitive currents obtained by subtraction. Panels *A3* and *B3* highlight the activation phases of control and Ni^{2+}-resistant currents, normalized to their peak amplitudes, over an expanded time scale (calibration bar: 5 msec). The insets show normalized Ni^{2+}-resistant and Ni^{2+}-sensitive currents superimposed (same time span as in the main panels). Current sampling interval was 50 μsec.

rent amplitude by ~43% on average (*see below*). In addition, residual I_{Ba}s consistently appeared to activate substantially more slowly than control currents. This is better illustrated in panels *A3* and *B3* of Fig. 1, where total and residual currents are shown, over an expanded time scale, normalized to their maximal amplitudes. As a consequence, Ni^{2+}-sensitive currents, obtained by subtraction (Fig. 1*A2* and *B2*), appeared to activate substantially faster than both control and Ni^{2+}-resistant currents (Fig. 1*A3* and *B3*, insets). In some cases, the difference between control and residual current activation speed was such that subtracted currents displayed a transient, remarkably fast-decaying component at their beginning (Fig. 1*B2*, arrow).

Both effects of Ni^{2+} were readily reversible upon washout (Fig. 1*A1* and *B1*).

Ni^{2+} Reduces I_{Ba} Activation Speed over a Wide Range of Test Potentials

The above-described effect of Ni^{2+} on the activation kinetics of residual I_{Ba}s was better quantified by performing exponential fittings of the activation phases of currents evoked over a wide range of test potentials. The activation kinetics of the currents under study were consistently biexponential. In order to provide a synthetic description of the effects of Ni^{2+} on I_{Ba} activation speed, we identified the following parameter:

$$\bar{\tau}_{act} = \tau_{act1} \cdot A_1/(A_1 + A_2) + \tau_{act2} \cdot A_2/(A_1 + A_2) \qquad (4)$$

which effectively lumps together all of the important kinetic parameters (time constants and relative amplitude coefficients), thus providing a useful operative quantification of the overall current activation speed.

Figure 2*A* shows normalized I_{Ba}s recorded at various test potentials in a representative neuron, both in control conditions and during application of 50-μM Ni^{2+}, along with biexponential fittings of their activation phases. The values of the lumped activation time constant, $\bar{\tau}_{act}$, are also shown. It is apparent that Ni^{2+} reduced current activation rate over the whole voltage range of I_{Ba} activation. Average data are shown in panels *B1–5*. $\bar{\tau}_{act}$ was consistently increased by Ni^{2+} (Fig. 2*B1*). This effect

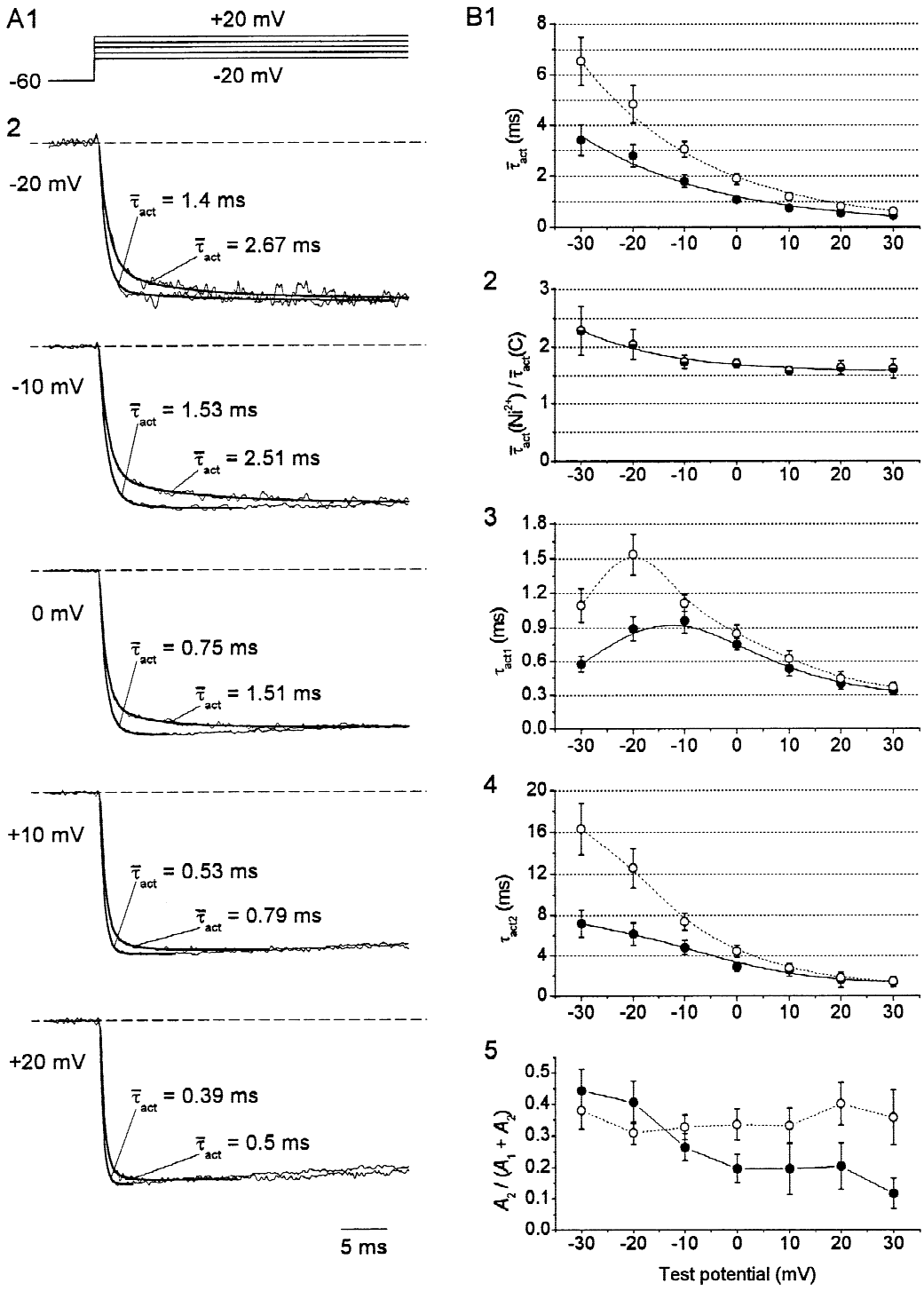

Fig. 2. Ni^{2+} reduces I_{Ba} activation speed over a wide range of test potentials. (*A*) Detail of the activation phases of I_{Ba}s recorded in a representative neuron (cell B9210), in response to step depolarizations at various voltage levels (see the voltage protocol in *A1*), before and during application of 50-μM Ni^{2+}. Currents have been normalized to their peak amplitudes. The slower-activating currents are those recorded in the presence of Ni^{2+}. Current sampling interval was 50 μsec. Enhanced lines are biexponential best fittings to current activation phases. The values of the lumped activation time constant ($\bar{\tau}_{act}$; *see* text for details) are also shown. (*B*) Average plots of the voltage dependence of kinetic parameters returned by biexponential fittings of I_{Ba} activation phase: lumped activation time constant, $\bar{\tau}_{act}$ (*B1*), individual fast and slow activation time constants, τ_{act1} and τ_{act2} (*B3* and *B4*, respectively), relative amplitude coefficient of the slow exponential component (*B5*). Filled symbols: control; empty symbols: 50-μM Ni^{2+}. Smooth lines in *B1* are monoexponential best fittings to $\bar{\tau}_{act}$ data points, obtained using the function described in the last section of the Results. Panel *B2* shows the average values of the ratio of $\bar{\tau}_{act}$ measured in Ni^{2+} to $\bar{\tau}_{act}$ measured in control conditions. $n = 15$ throughout.

was weakly dependent on test voltage, since the ratio of $\bar{\tau}_{act}$ in Ni^{2+} to $\bar{\tau}_{act}$ in control conditions [$\bar{\tau}_{act}(Ni^{2+})/\bar{\tau}_{act}(C)$] averaged ~2.28 close to I_{Ba} activation threshold, and reached a steady value of ~1.65 at the most positive test potentials used (+10 to +30 mV) (Fig. 2*B2*). Both individual time constants of I_{Ba} activation (τ_{act1} and τ_{act2}) were consistently slowed down by Ni^{2+} over the whole voltage range of current activation (Fig. 2*B3* and *B4*). Moreover, the relative amplitude coefficient of the slow activation component [$A_2/(A_1 + A_2)$] consistently decreased at increasingly positive voltage levels in the unblocked currents, whereas during Ni^{2+} application it maintained a relatively steady, high value regardless by the test potential (Fig. 2*B5*). All of these individual effects, hence, contributed to the global slowing of residual I_{Ba} activation kinetics carried out by Ni^{2+} and synthetically described by $\bar{\tau}_{act}$.

Slowing of Residual I_{Ba} Activation Kinetics by Ni^{2+} is Not Due to Block of a Fast-Activating Current Component

The slow activation kinetics observed in the residual currents recorded during Ni^{2+} application can, in principle, be explained in two different ways: (i) Ni^{2+} preferentially blocks a fast-activating current component, thus revealing an underlying slower-activating current; (ii) Ni^{2+} actually reduces the activation speed of whole-cell I_{Ba}s, with a mechanism to be established. To test the former hypothesis, we verified whether pharmacological component(s) characterized by slower or faster activation kinetics than other components could be isolated from the currents under study.

We first characterized the activation properties of the individual pharmacological components that constitute the slowly-decaying HVA I_{Ba}s under study. The current fractions specifically sensitive to saturating concentrations of nifedipine (10 μM), ω-conotoxin GVIA (0.5 μM), and ω-conotoxin MVIIC (1 μM) were identified as L-, N-, and P/Q-type components, respectively, whereas the residual current recorded in the simultaneous presence of all of the above blockers was identified as R-type. Figure 3 illustrates the results obtained in a typical cell in which the individual current components were pharmacologically dissected. From the superimposed, normalized current traces (Fig. 3*B*) it is apparent that none of these components displayed activation kinetics significantly different from those of total, control currents. In six cells, the lumped activation time constant, $\bar{\tau}_{act}$, was measured in each pharmacological current component at 0 mV, and averaged 1.091 ± 0.10 msec for the L-type current, 1.065 ± 0.069 msec for the N-type current, 1.049 ± 0.109 msec for the P/Q-type current, and 0.988 ± 0.141 msec for the R-type current. None of these values was significantly different from that derived from the corresponding, total I_{Ba}s (1.072 ± 0.089 msec). Hence, no specific current component matching the activation properties of the "Ni^{2+}-resistant" or "Ni^{2+}-sensitive" currents was found in the cells under study.

In addition, we investigated whether Ni^{2+} application could reduce the activation speed of residual currents in different pharmacological I_{Ba} components. Figure 4*A* shows the results of a typical experiment in which the effects of 50-μM Ni^{2+} were tested on both the R-type and the non-R-type current components of the neurons under study. The activation phase of the "Ni^{2+}-sensitive" portion of R-type currents, obtained by subtraction, was remarkably faster than in residual, R-type currents (Fig. 4*B2*). The same was also true for the subtracted non-R-type current component (which is mainly composed of an L- and an N-type current component in our cell system) (Fig. 4*B1*). Very similar results were obtained in three other neurons. These data prompt the conclusion that Ni^{2+} ions reduce the activation speed of residual currents in various pharmacological I_{Ba} components, in none of which can subcomponents characterized by heterogeneous activation kinetics be demonstrated.

The Blocking Effect of Ni^{2+} is Not Voltage Dependent over the Voltage Range of I_{Ba} Activation

Once the possibility that Ni^{2+} preferentially inhibits a fast-activating current component has been ruled out, we can conclude that Ni^{2+} exerts a real slowing effect on I_{Ba} activation kinetics. Such an effect can, in turn, be the result of two different mechanisms: (i) upon depolarization, the block[1] exerted by Ni^{2+} on Ca^{2+} channels is partly relieved with relatively slow kinetics, which accounts for an apparent decrease of the activation speed of residual I_{Ba}s; (ii) Ni^{2+} decreases the speed of Ca^{2+}-channel transitions from closed to open states, with a mechanism that could be independent of the blocking action in itself.

The first hypothesis implies that the blocking action of Ni^{2+} is stronger at negative than at more positive voltage levels. This would not be unexpected for an extracellular cation that blocks the Ca^{2+}-channel pore by occupying a site located within the permeation path, and thus experiences the intramembranal electric field. In

[1] When we use the term "block" alone, we do not necessarily mean channel-pore obstruction, but rather any possible mechanism that would result in partial or complete inhibition of I_{Ba}s throughout their whole *I-V* relationship, including stabilization of nonconducting channel states. When reference is made specifically to a mechanism implying obstruction of the permeation path, the expression "channel-pore block", or an equivalent one, is used.

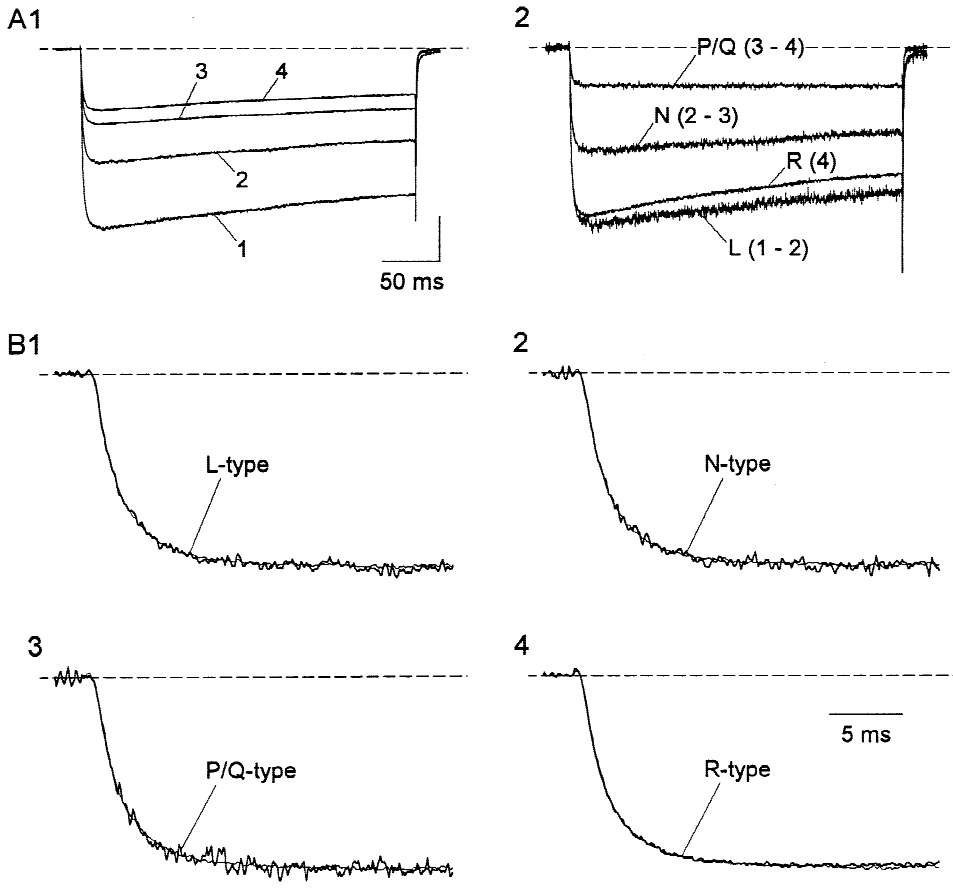

Fig. 3. L-, N-, P/Q-, and R-type currents activate with kinetics similar to that of total currents in slowly decaying I_{Ba}s. (*A*) Effects of the application of specific Ca^{2+}-channel blockers on I_{Ba}s recorded at the test potential of 0 mV in a representative neuron (cell A9127). Panel *A1* shows the currents recorded in control conditions (1) and during application of 10-μM nifedipine (2), 10-μM nifedipine + 0.5-μM ω-conotoxin GVIA (3), and 10-μM nifedipine + 0.5-μM ω-conotoxin GVIA + 1-μM ω-conotoxin MVIIC (4). Each trace is the average of 4–8 sweeps. Panel *A2* shows the single pharmacological current components. The L-, N-, and P/Q-type components have been isolated by subtraction from the traces indicated in parentheses. *y*-axis scale: 200 pA in *A1*, 74 pA in *A2*. (*B*) The current traces illustrated in panel *A2*, each of which corresponds to a single pharmacological I_{Ba} component, have been normalized to their peak amplitudes and expanded in the time scale to highlight their activation phases. Each panel shows a single pharmacological component (thicker line) superimposed to the normalized control current of panel *A1* (thinner line). Note that the time scale is the same as in Fig. 1*A3* and *B3*. Current sampling interval was 50 μsec throughout.

this case, membrane depolarization would oppose the cation to penetrate into the channel pore (*see* Hille, 1992). An alternative (or additional) possibility is that Ni^{2+}, rather than obstructing the permeation path, stabilizes closed states in a voltage-dependent manner, which would be possible if the Ni^{2+}/channel interaction is opposed in the presence of channel conformational changes promoted by depolarization. Under each one of the above assumptions, we can expect that the steady-state blocking effect of Ni^{2+} on I_{Ba}s is progressively smaller with increasingly positive levels of the voltage pulses used to elicit I_{Ba}s themselves.

To test this possibility, we used the experimental approach illustrated in Fig. 5. I_{Ba}s were evoked, both in control conditions and during application of 50-μM Ni^{2+}, over a wide range of test voltages (Fig. 5*A*). I_{Ba} peak amplitudes were then measured, and the corresponding permeability values (P_{Ba}) were calculated on the basis of the Goldman equation, as explained in Materials and Methods. If the Ni^{2+} blocking effect decreases with depolarization over the voltage range of I_{Ba} activation, we would expect a higher percentage of Ni^{2+}-dependent P_{Ba} inhibition close to the conductance's threshold rather than at more positive voltage levels, and, consequently, an overall shift in the positive direction of P_{Ba} voltage dependence of activation. The inset in Fig. 5*A* shows the plots of P_{Ba} voltage dependence of activation obtained in a representative neuron. The plot relating to control currents was fitted with a single Boltzmann function, with $V_{1/2} = +0.3$ mV and $k = -6.5$ mV. The plot derived from Ni^{2+}-inhibited currents had a very similar behavior, and could be faithfully described by the same Boltzmann function scaled down by a factor of 0.63. Average, normalized $P_{Ba}(V)$ plots are shown in Fig. 5*B*. It is apparent

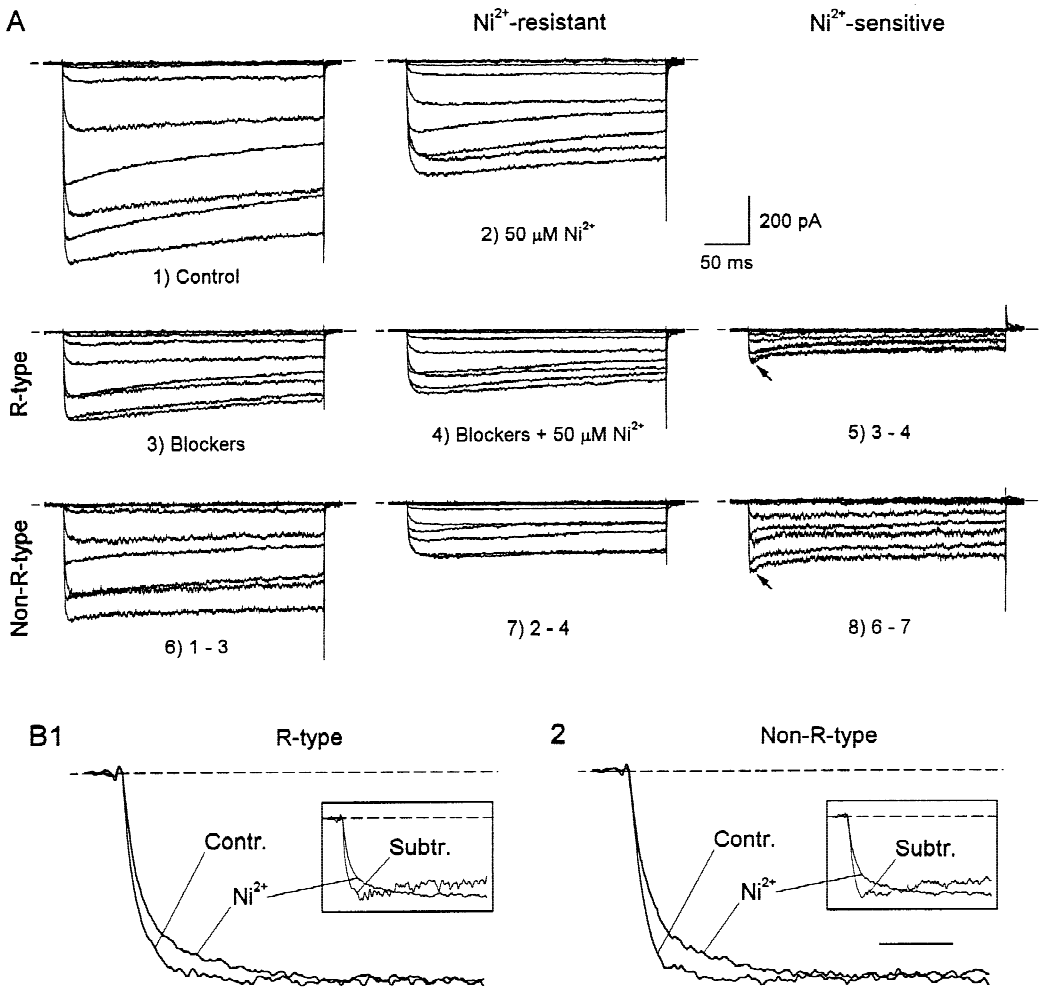

Fig. 4. Ni^{2+} decreases the activation speed of both R- and non-R-type currents. (*A*) I_{Ba}s recorded at various test potentials in a representative neuron (cell A9420). The voltage protocol applied was the same as shown in Fig. 5*A1*. The trace families marked 1 to 4 are original current recordings, those marked 5 to 8 have been obtained by subtraction. In the latter cases, the currents used for subtraction are indicated. Currents were recorded in control conditions (1), in the presence of 50-μM Ni^{2+} (2), in the presence of 10-μM nifedipine + 0.5-μM ω-conotoxin GVIA + 1-μM ω-conotoxin MVIIC after the washout of Ni^{2+} ("blockers": 3), and in the presence of both Ni^{2+} and the above-described organic-blocker cocktail (4). The arrows point at the transient, fast-decaying component observed at the beginning of Ni^{2+}-sensitive currents obtained by subtraction. (*B*) The activation phase of control and Ni^{2+}-resistant currents activated at +10 mV, normalized to their peak amplitudes, is shown over an expanded time scale (calibration bar: 5 msec), for both R-type (*B1*) and non-R-type (*B2*) currents. The insets show normalized Ni^{2+}-resistant and Ni^{2+}-sensitive currents superimposed (same time span as in the main panels). Current sampling interval was 50 μsec.

that Ni^{2+} caused neither a rightward shift in P_{Ba} voltage dependence of activation, nor a change in the curve shape and slope. $V_{1/2}$ and k values derived from Boltzmann fittings of individual plots averaged −6.7 ± 1.4 mV and −6.5 ± 0.2 mV in control currents, respectively, and −7.4 ± 1.4 mV and −6.6 ± 0.2 mV in residual currents, respectively. The differences were not statistically significant ($P < 0.3$ and $P < 0.4$, respectively, according to the *t*-test for paired data). To further illustrate the lack of voltage dependence of Ni^{2+} blocking effect over the voltage range of I_{Ba} activation, we calculated the fractional current reduction caused by 50-μM Ni^{2+} at two different, distant voltage levels (−30 and +10 mV). The degree of Ni^{2+}-dependent I_{Ba} inhibition proved not to be lower at +10 mV than at −30 mV (Fig. 5*C*).

Slowing of I_{Ba} Activation Kinetics by Ni^{2+} is not Due to a Voltage- and Time-Dependent Unblocking Mechanism

So far, we have demonstrated that Ni^{2+} block of I_{Ba}s is not voltage dependent over the examined voltage range of I_{Ba} activation. Yet, this is not a final demonstration that Ni^{2+} does not slow current activation kinetics with a mechanism involving voltage- and time-dependent relief

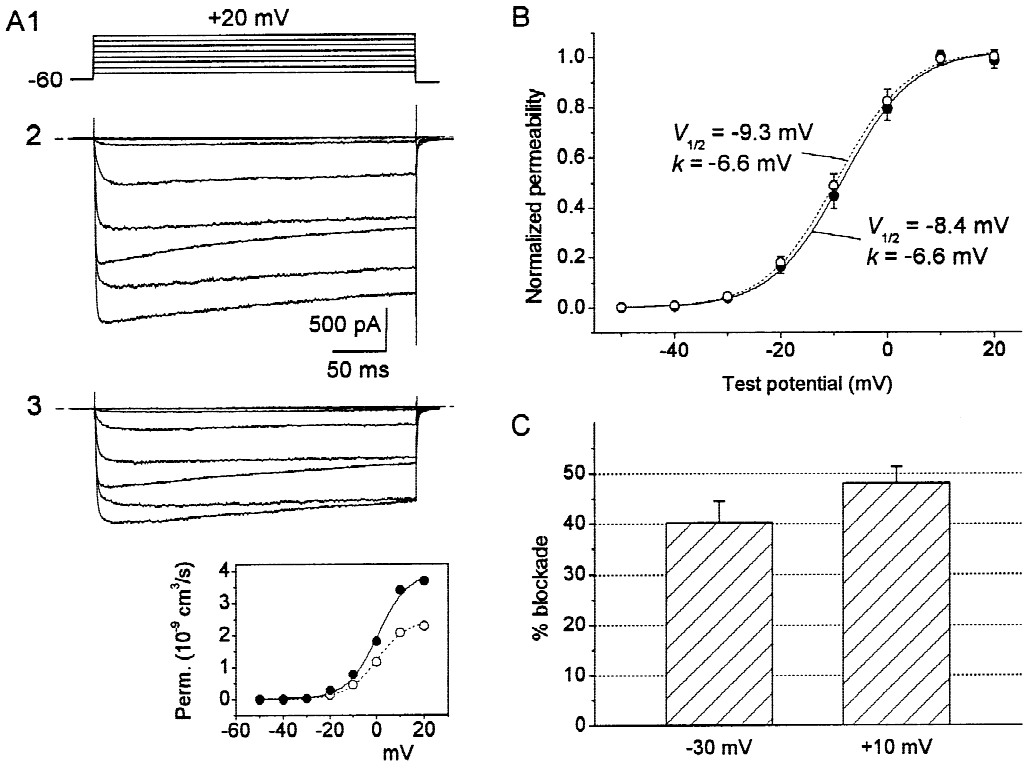

Fig. 5. Ni^{2+} does not modify the voltage dependence of activation of I_{Ba}. (*A*) I_{Ba}s recorded in a representative neuron (cell A9909), in response to step depolarizations at various voltage levels (*see* the voltage protocol in *A1*), before (*A2*) and during (*A3*) application of 50-μM Ni^{2+} (current sampling interval was 50 μsec). The inset in panel *A3* shows the plot of the voltage dependence of the underlying Ba^{2+} permeabilities (P_{Ba}s) derived from peak I_{Ba}s as explained in Materials and Methods. Filled symbols: control; empty symbols: 50-μM Ni^{2+}. The smooth, continuous line is the best Boltzmann fit to control data points, with $V_{1/2} = +0.3$ mV and $k = -6.5$ mV. The dotted line is the same Boltzmann fit as before, scaled down by a factor of 0.63 to show the perfect overlapping with data points related to residual currents in Ni^{2+}. (*B*) Average, normalized plots of the voltage dependence of P_{Ba} in control (filled symbols) and 50-μM Ni^{2+} (empty symbols) ($n = 22$). P_{Ba} values have been normalized to the maximal value in each cell, averaged among cells, and further normalized to the maximal value of the average plot. The smooth lines are the best Boltzmann fits to data points (fit parameters are also specified nearby). (*C*) Average bar diagram of the percent blocking effect of 50-μM Ni^{2+} on I_{Ba} peak amplitude at two different test potentials (−30 and +10 mV; $n = 22$).

from block, since an additional possibility has to be excluded before this conclusion can be drawn. Let us suppose that Ni^{2+} blocking action comprises two distinct components (for instance, on two different channel types or conformational states): the first component would be voltage independent in the examined voltage range, and would account for the steady-state blocking effect of Ni^{2+} on I_{Ba}s elicited by depolarizing pulses. The second component, instead, would be strongly voltage dependent, such that from −60 mV (the voltage level from which the test pulses we applied started) to −30/−20 mV (the voltage levels at which detectable I_{Ba}s start to be recorded) the relief from block would be nearly complete. In this case, the time-dependent clearance of the blocking ion upon depolarization would not change the final, total amount of channels unblocked in the voltage range of I_{Ba} activation. As a consequence, no modification of the $P_{Ba}(V)$ function would be detected in residual currents during Ni^{2+} application.

This possibility is indeed compatible with the classical theory on voltage-dependent channel-pore block (*see* Hille, 1992). In the simplest case, the channel permeation path can be schematized, from the standpoint of the permeating ion, as a one-dimension energetic profile which comprises at least one energy well (namely, a binding site) preceded and followed by two energy barriers (*see* Fig. 6*A*, inset). The migration speeds of the permeating ion to and from the binding site are regulated by specific rate constants (k_is in Fig. 6*A* inset). If we assume that both Ba^{2+} and Ni^{2+} compete, with different affinities, for the same binding site, and that the energetic barrier towards the intracellular side is virtually infinite for Ni^{2+}, the ratio between I_{Ba} amplitude after Ni^{2+} blockade [$I_{Ba}(Ni^{2+})$] and control I_{Ba} amplitude [$I_{Ba}(C)$] will be:

$$I_{Ba}(Ni^{2+})/I_{Ba}(C) = 1/\{1 + ([Ni^{2+}]_o \cdot h_1/h_{-1})/[1 + [Ba^{2+}]_o \cdot k_1/(k_{-1} + k_2)]\} \quad (5)$$

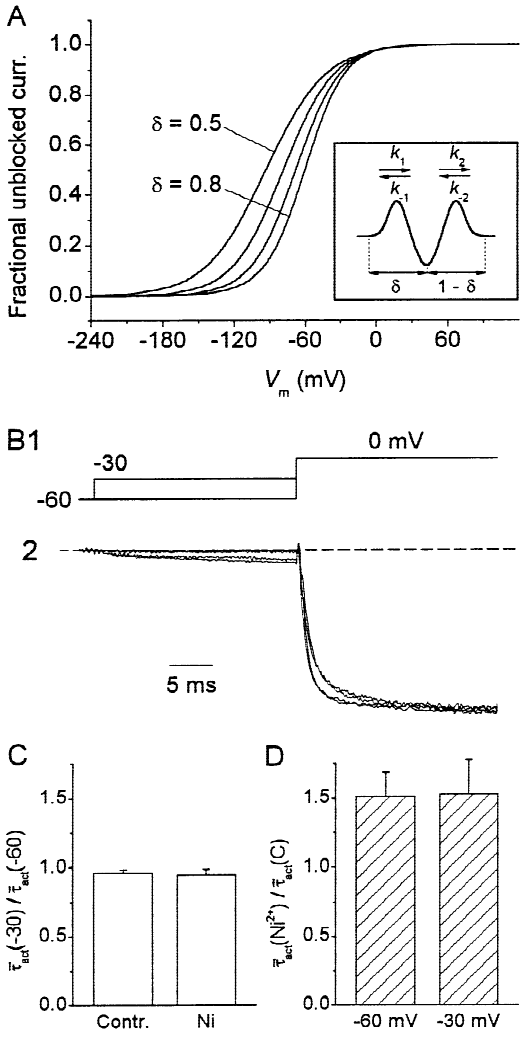

Fig. 6. Slowing of residual I_{Ba} during Ni^{2+} application is not affected by depolarizing prepulses at −30 mV. (*A*) Theoretical voltage dependence of the ratio $I_{Ba}(Ni^{2+})/I_{Ba}(C)$ (*see* text for details) calculated for a double-barrier energetic model of the Ca^{2+}-channel permeation path (inset). The equations applied for calculations are Eqs. 5 through 8 given in the text. The numeric values used for individual parameters were: $k_{-1}'/k_1' = 100 \times 10^3$ M^{-1}, $k_2'/k_1' = 100 \times 10^3$ M^{-1}, $h_1'/k_1' = 0.5$, $h_{-1}'/k_1' = 1 \times 10^3$ M^{-1}, $h_2'/k_1' = 0$ M^{-1}, $[Ba^{2+}]_o = 5 \times 10^{-3}$ M, $[Ni^{2+}]_o = 50 \times 10^{-6}$ M. Curves for various values of δ (*see text*) are shown (δ = 0.5, 0.6, 0.7, 0.8). (*B*) Experimental protocol used for testing the effect of depolarizing pre-steps on Ni^{2+}-induced slowing of I_{Ba} activation kinetics. Panel *B1* illustrates the applied voltage protocol, panel *B2* shows I_{Ba}s recorded in a representative neuron (cell B9909), both in the absence and in the presence (slower-activating currents) of 50-μM Ni^{2+}. Currents have been normalized to their peak values. Current sampling interval was 20 μsec. (*C*) Lack of effects of the 25-msec conditioning prepulse at −30 mV on I_{Ba} activation kinetics. The lumped activation time constant, $\bar{\tau}_{act}$, was measured in the currents recorded in each cell without $[\bar{\tau}_{act}(-60)]$ or with $[\bar{\tau}_{act}(-30)]$ application of the prepulse at −30 mV. The bar diagram shows the average ratio, $\bar{\tau}_{act}(-30)/\bar{\tau}_{act}(-60)$, for both control currents and residual currents after Ni^{2+} delivery ($n = 6$). (*D*) Lack of effects of the 25-msec conditioning prepulse at −30 mV on Ni^{2+}-induced decrease of I_{Ba} activation speed. In each cell, the ratio between $\bar{\tau}_{act}$ of residual currents during Ni^{2+} application $[\bar{\tau}_{act}(Ni^{2+})]$ and $\bar{\tau}_{act}$ of control currents $[\bar{\tau}_{act}(C)]$ was measured. The bar diagram shows the average ratio, $\bar{\tau}_{act}(Ni^{2+})/\bar{\tau}_{act}(C)$, for currents recorded without (−60) or with (−30) application of the prepulse at −30 mV ($n = 6$).

where k_is are the rate constants for Ba^{2+}, h_is are the rate constants for Ni^{2+} and $[S]_o$ are the concentrations of the ions in the extracellular side. h_2 (according to the above hypothesis on the energetic barrier for Ni^{2+} towards the internal side), $[Ba^{2+}]_i$ and $[Ni^{2+}]_i$ have been assumed to be zero. Insofar as the binding site is located inside the intramembranal electric field, each one of the rate constants is voltage dependent (*see* Hille, 1992). If we assume that the intramembranal electric field is constant, and that the energy barriers and well are symmetrical in width along the *x* axis, we have, for example:

$$\begin{aligned} k_1 &= k_1' \cdot \exp(-\delta V \cdot zF/2RT), \\ k_{-1} &= k_{-1}' \cdot \exp(\delta V \cdot zF/2RT), \\ k_2 &= k_2' \cdot \exp[-(1-\delta)V \cdot zF/2RT] \end{aligned} \qquad (6\text{–}8)$$

where δ is the fraction of the membrane width (from its extracellular surface) at which the binding site is located, and *z* is the ionic valence (2 in our case).

Figure 6*A* shows the voltage dependence of the ratio $I_{Ba}(Ni^{2+})/I_{Ba}(C)$ calculated, on the basis of Eq. 5, Eqs. 6–8 and the equivalent equations describing $h_i(V)$, for particular values of k_i' and h_i' relative to k_i' (*see* Fig. 6 legend). It is apparent that from −60 to −30/−20 mV a significant relief from Ni^{2+} block up to nearly complete levels can take place, especially for high values of δ.

If the above-illustrated theoretical situation indeed applies to the real case under study, we would expect that virtually no voltage- and time-dependent relief from Ni^{2+} block, and hence no slowing of I_{Ba} activation kinetics, is produced when the depolarizing test pulses are applied starting from −30 mV rather than −60 mV. We tested this possibility by performing experiments exemplified in Fig. 6*B*. I_{Ba}s were evoked, both in control and during application of 50-μM Ni^{2+}, by test pulses at 0 mV delivered either from the usual level of −60 mV, or after a conditioning prepulse at −30 mV (Fig. 6*B1*). The duration of this prepulse was 25 msec, namely ~4 times the average $\bar{\tau}_{act}$ observed under Ni^{2+} at the same voltage level. The application of prepulses of this duration did not significantly modify the activation kinetics of control I_{Ba}s elicited at 0 mV (*see* Fig. 6*C*). The current traces of Fig. 6*B2* clearly show that no detectable reduction of the slowing action exerted by Ni^{2+} on I_{Ba} activation kinetics was caused by the depolarizing prepulse at −30 mV. The average data are illustrated in Fig. 6*D*, which shows that the ratio between $\bar{\tau}_{act}$ of residual currents during Ni^{2+} application and $\bar{\tau}_{act}$ of control currents was virtually unchanged by the conditioning depolarization at −30 mV. These results provide a conclusive demonstration that the

decrease in I_{Ba} activation speed carried out by Ni^{2+} is not due to a voltage- and time-dependent unblocking mechanism.

Ni^{2+} Decreases I_{Ba} Deactivation Speed

We further examined whether Ni^{2+}, besides decreasing I_{Ba} activation speed, also affects I_{Ba} deactivation kinetics upon repolarization. The voltage protocol routinely applied for this purpose is illustrated in Fig. 7*A1*. Fifteen-msec test pulses delivered to elicit I_{Ba}s were followed by step repolarizations at voltage levels variable from −20 to −60 mV. In these experiments, the 2-sec conditioning prepulse and the test pulse were set at −50 mV and −10 mV, respectively, so as to reduce the current size and thereby optimize the clamp control of tail currents. Figure 7*A2* shows the currents recorded in a representative neuron in response of such voltage protocol, both in the absence and presence of 50-μM Ni^{2+}. Currents are shown normalized to the peak amplitude of the tail currents resulting from step repolarization. The decay rate of tail currents was clearly slowed down by Ni^{2+} in the whole voltage range explored. Such slowing effect was readily reversible upon Ni^{2+} washout (*see* Fig. 7*A2*, inset). The decay phase of tail currents consistently followed a biexponential time course. The average data on the parameters returned by biexponential fittings of tail currents are shown in Fig. 7*B1–4*. Ni^{2-} application consistently increased the lumped deactivation time constant, $\bar{\tau}_{deact}$ (calculated in the same way as the lumped activation time constant, $\bar{\tau}_{act}$: *see above*, Eq. 4), by ~1.2–1.5 times, depending on the voltage level (Fig. 7*B1*). Both individual time constants of deactivation, τ_{deact1} and τ_{deact2}, were increased by Ni^{2+} in the voltage range considered (Fig. 7*B2, 3*), whereas the relative amplitudes of the two exponential components were not significantly modified (Fig. 7*B4*).

We also examined the slowing action of 50-μM Ni^{2+} on tail currents elicited after prolonged depolarizing test pulses. The protocol used in these experiments is shown in Fig. 8*A1*: three-hundred-msec voltage steps at −10 or 0 mV delivered to evoke I_{Ba}s were followed by a repolarizing step at −60 mV. Again, the decay phase of the resultant tail currents was markedly slowed by Ni^{2+} application, in a readily reversible manner (Fig. 8*A2*, inset). Figure 8*B* compares the average effects of Ni^{2+} on $\bar{\tau}_{deact}$s of tail currents evoked after long (300-msec) depolarizing pulses with those on $\bar{\tau}_{deact}$s of tail currents evoked after short (15-msec) pulses (in both cases, with repolarizing steps at −60 mV). The slowing action exerted by Ni^{2+} on tail-current $\bar{\tau}_{deact}$s was much more pronounced after long than after short depolarizing pulses. The ratio of $\bar{\tau}_{deact}$ in Ni^{2+} to $\bar{\tau}_{deact}$ in control conditions was 1.76 ± 0.11 after 300-msec pulses *vs.* 1.34 ± 0.03 after 15-msec pulses ($P < 0.05$). These findings suggest that Ni^{2+} may decrease the rates of open-to-closed channel transitions more effectively starting from open states that are favored by long-lasting depolarizations. In this case, Ni^{2+} effects on channel kinetics would also be state dependent (*see* Discussion).

It is worth to note that the decrease of I_{Ba} deactivation speed observed during Ni^{2+} application is further evidence that Ni^{2+} modifies I_{Ba} kinetics independently of a mechanism of voltage- and time-dependent relief from block. Under the assumption that Ni^{2+} acts as a channel-pore blocker, and that depolarizations over the voltage range of I_{Ba} activation are associated with substantial degrees of relief from block, one would expect that, upon repolarization, the tendency of Ni^{2+} to re-occlude open channels would create an additional escape path from conducting to nonconducting states, thus accelerating, rather than slowing, the apparent deactivation kinetics. The simplest kinetic scheme would be:

$$\begin{array}{l} \quad\quad\quad O \overset{s_1}{\rightarrow} C \\ +Ni^{2+} \downarrow \; s_2 \\ \quad\quad\quad O \cdot Ni^{2+}\ \text{(blocked)} \end{array} \qquad \text{(Scheme 1)}$$

in which case τ_{deact} under Ni^{2+} would equal $1/(s_1 + s_2)$, a quantity that cannot be higher than $1/s_1$, namely τ_{deact} in control conditions. As well, under the hypothesis that Ni^{2+} inhibits I_{Ba}s by stabilizing nonconducting states and that this effect is opposed upon depolarization, either no change or an acceleration of repolarization-induced tail currents would be expected.

Concentration Dependence of the Effects of Ni^{2+} on I_{Ba} Amplitude and Time Course of Activation

All of the above-illustrated results on the effects of Ni^{2+} on I_{Ba}s were obtained after application of 50-μM $NiCl_2$. We further investigated the concentration dependence of the effects of Ni^{2+} both on I_{Ba} amplitude and activation kinetics. Figure 9*A1* shows the results of a typical experiment in which Ni^{2+} was delivered at increasing concentrations (from 5 to 150 μM). The inhibitory effect of Ni^{2+} on I_{Ba} amplitude was progressively higher with the increasing Ni^{2+} concentrations applied. The concentration dependence of the Ni^{2+} blocking effect is illustrated by the average plots of Fig. 9*B* and *C*. I_{Ba} amplitude was measured at the peak of the *I-V* relationship, and its fractional inhibition was plotted as a function of extracellular Ni^{2+} concentration ($[Ni^{2+}]_o$). This plot could be properly fitted with a Langmuir adsorption isotherm function, in the form:

$$[I_{Ba}(C) - I_{Ba}(Ni^{2+})]/I_{Ba}(C) = [Ni^{2+}]^n/(K_D + [Ni^{2+}]^n)$$

where $I_{Ba}(C)$ and $I_{Ba}(Ni^{2+})$ are the current amplitudes in control and under Ni^{2+}, respectively, K_D is the apparent dissociation constant for the Ca^{2+} channel-Ni^{2+} interaction, and n is a Hill coefficient indicating the number of

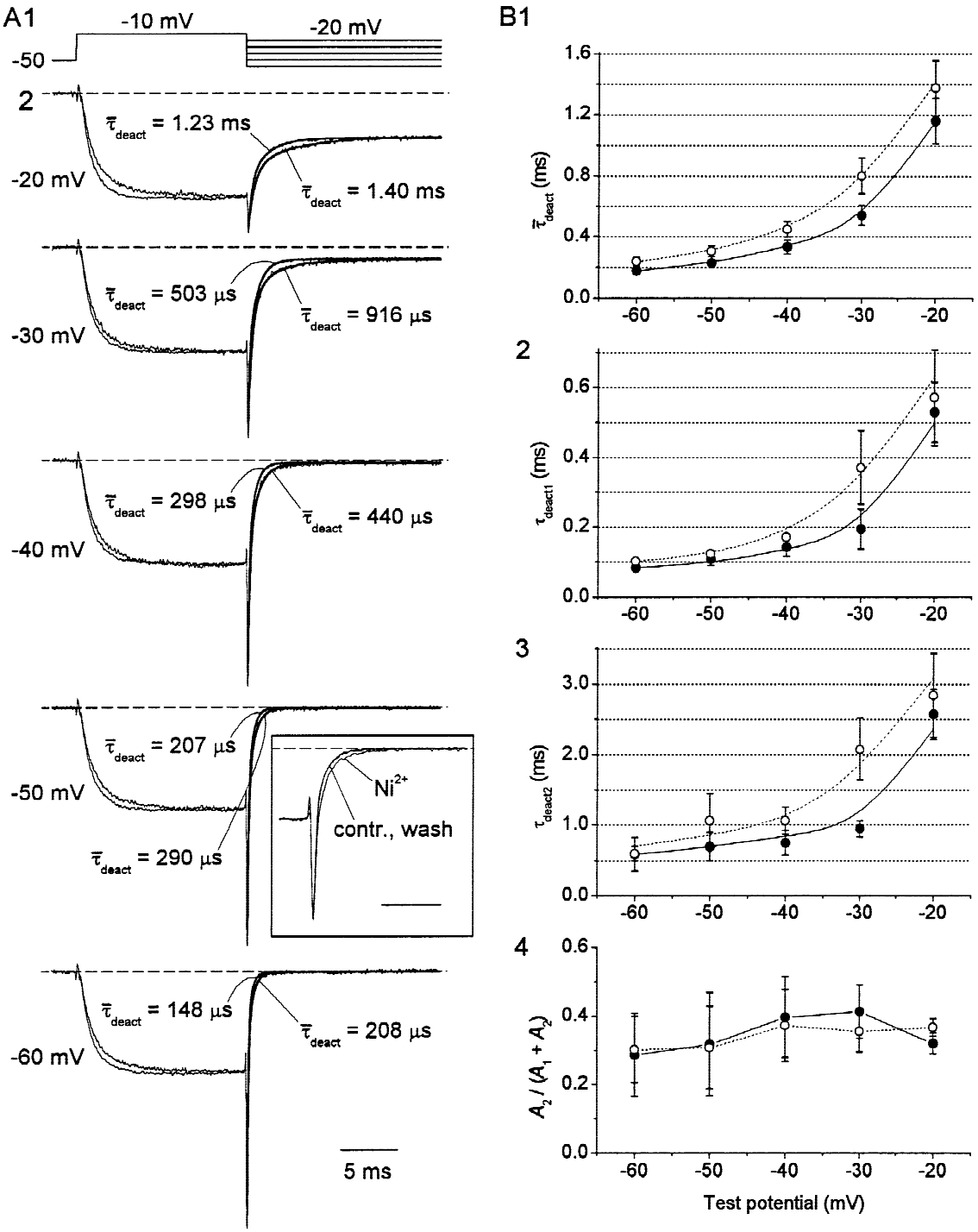

Fig. 7. Ni^{2+} slows I_{Ba} tail currents after short depolarizing pulses. (*A*) I_{Ba}s recorded in a representative neuron (cell C0127) in response to a fixed depolarizing step at −10 mV, followed by repolarizing steps at variable voltage levels (*see* the voltage protocol in *A1*), before and during application of 50-μM Ni^{2+}. The slower-activating and deactivating currents are those recorded in the presence of Ni^{2+}. Currents have been normalized to the peak amplitudes of tail currents (I_{tail}s) elicited upon step depolarization. Current sampling interval was 20 μsec. Enhanced lines are biexponential best fittings to I_{tail} deactivation phases. The values of the lumped deactivation time constant ($\bar{\tau}_{deact}$; *see* text for details) are also shown. The inset is a highlight, over an expanded time scale (calibration bar: 2 msec), of I_{tail}s recorded at −50 mV before and during application of 50-μM Ni^{2+}, and after the washout of Ni^{2+}. (*B*) Average plots of the voltage dependence of kinetic parameters returned by biexponential fittings of I_{tail} deactivation phase; lumped deactivation time constant, $\bar{\tau}_{deact}$ (*B1*), individual fast and slow deactivation time constants, τ_{deact1} and τ_{deact2} (*B2* and *B3*, respectively), relative amplitude coefficient of the slow exponential component (*B4*). Filled symbols: control; empty symbols: 50-μM Ni^{2+} ($n = 4$ throughout).

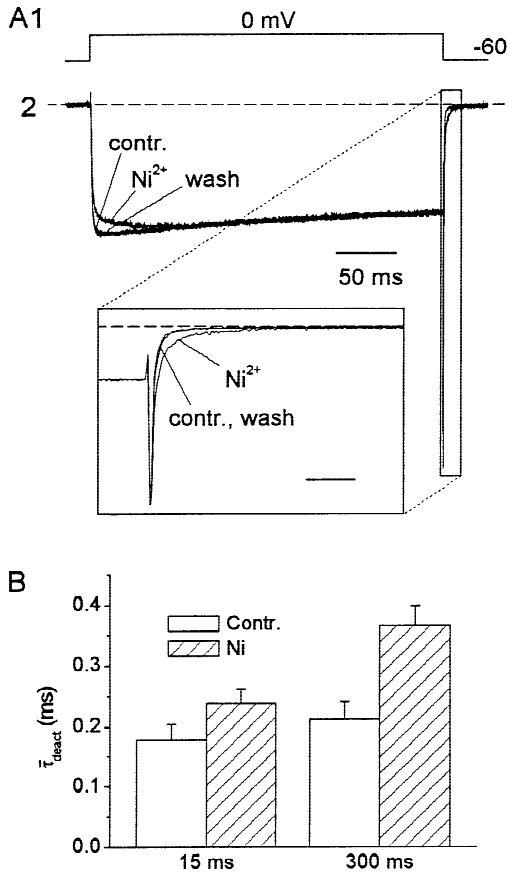

Fig. 8. Tail currents are slowed by Ni^{2+} even more prominently after prolonged depolarizations. (*A*) I_{Ba}s recorded in a representative neuron (cell A9222) in response to a 300-msec depolarizing step at 0 mV, followed by a repolarizing steps at −60 mV (see the voltage protocol in *A1*), before and during application of 50-μM Ni^{2+}, and after the washout of Ni^{2+}. Currents have been normalized to the peak amplitudes of tail currents. Current sampling interval was 50 μsec. The inset is a highlight of I_{tail} deactivation, shown over an expanded time scale (calibration bar: 3 msec). (*B*) Average bar diagram of the effects of 50-μM Ni^{2+} on the lumped deactivation time constant, $\bar{\tau}_{deact}$, of I_{tail}s elicited at −60 mV after depolarizing pulses of 15 or 300 msec.

Ni^{2+} ions that must bind to each Ca^{2+} channel for the blocking effect to be reached. The fitting of the average plot returned a K_D of 87.8 μM and an n coefficient very close to 1 (1.088), with an EC_{50} ($=K_D^{1/n}$) of 61.1 μM.

The reduction of I_{Ba} activation speed carried out by Ni^{2+} also increased in a concentration-dependent manner. However, the effect of raising $[Ni^{2+}]_o$ from 50 to 150 μM was not as prominent on I_{Ba} activation speed (Fig. 9*A2*) as on I_{Ba} amplitude (Fig. 9*A1*). To quantify the concentration dependence of the slowing of I_{Ba} activation kinetics carried out by Ni^{2+}, the ratio $[\bar{\tau}_{act}(Ni^{2+}) - \bar{\tau}_{act}(C)]/\bar{\tau}_{act}(C)$ was determined, from the currents recorded at 0 mV, for different Ni^{2+} concentrations, and normalized to the maximal value observed in each cell. An average plot of the above quantity as a function of $[Ni^{2+}]_o$ was then constructed (Fig. 9*D*). Overall, the plot appeared to be significantly shifted leftwards along the x axis as compared to that describing I_{Ba} fractional inhibition as a function of $[Ni^{2+}]_o$. Again, the plot was properly fitted by a Langmuir adsorption isotherm (*see above*). The fitting returned a K_D of 185.0 μM and an n coefficient of 1.73, with an EC_{50} of 20.5 μM. The difference between the latter n coefficient and that obtained from the plot of I_{Ba}-amplitude inhibition as a function of $[Ni^{2+}]_o$ was statistically significant ($P = 0.0292$, one-tail Student's t test). The theoretical functions describing the dependence on $[Ni^{2+}]_o$ of the fractional effects of the cation on I_{Ba} amplitude and activation kinetics are directly compared in Fig. 9*E*, which highlights the differences, in terms of EC_{50} and overall shape, of the two curves. The fact that the Langmuir fitting of the plot describing the ratio $[\bar{\tau}_{act}(Ni^{2+}) - \bar{\tau}_{act}(C)]/\bar{\tau}_{act}(C)$ as a function of $[Ni^{2+}]_o$ returned a Hill coefficient closer to 2 than 1 strongly suggests that at least another binding site, implicated in the Ni^{2+}-dependent decrease of I_{Ba} activation speed, must exist in addition to that whose occupancy results in I_{Ba} block.

Strong Depolarizations Partly Relieve Ni^{2+}-Dependent Block of I_{Ba}s

We have demonstrated above that the inhibitory action exerted by Ni^{2+} on I_{Ba} amplitude is not significantly voltage dependent over the potential range explored with the voltage-clamp protocols routinely used in our study. However, if the mechanism of such blocking effect consists in an obstruction of the channel permeation path due to Ni^{2+} binding to the pore interior, the classical theory on channel block predicts that some degree of voltage dependence of the block, even if possibly weak, *should* exist over some voltage range. Since Ni^{2+} has already been shown to behave as a Ca^{2+}-channel pore blocker in other experimental models (Chesnoy-Marchais, 1985; Winegar et al., 1991), we investigated the effects of strong depolarizations on Ni^{2+}-dependent inhibition of I_{Ba} amplitude in the cells under study. The protocol used for this purpose and the current traces obtained in a representative neuron are shown in Fig. 10*A*. The voltage protocol consisted of 15-msec depolarizing pulses at +60 mV, followed by step repolarizations to variable voltage levels (from +20 to −60 mV). The initial, strong depolarization activated Ca^{2+} channels, but the ensuing currents were virtually undetectable due to the very low driving force for Ba^{2+} at such a positive voltage level. The number of Ca^{2+} channels recruited to an open and conductive state was rather reported by the amplitude of the tail currents (I_{tail}) elicited by step repolarizations. I_{tail}s were recorded both in control conditions and during Ni^{2+} application, and I_{tail} peak amplitudes were plotted as a function of command voltage (Fig. 10*B*). Over the

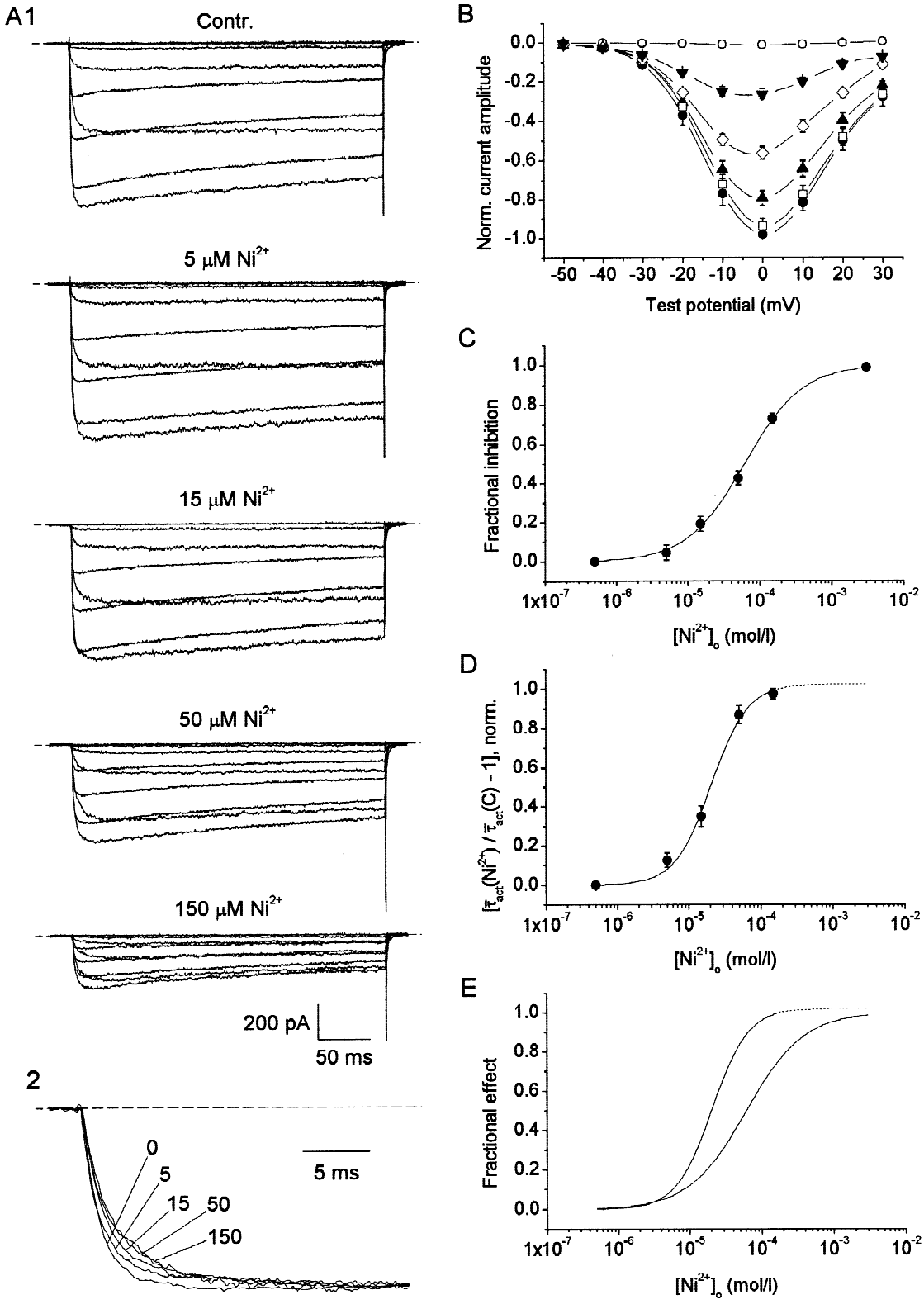
A1
Contr.
5 μM Ni2+
15 μM Ni2+
50 μM Ni2+
150 μM Ni2+
200 pA
50 ms
2
0
5
15
50
150
5 ms
B
Norm. current amplitude
Test potential (mV)
C
Fractional inhibition
[Ni2+]o (mol/l)
D
[τact(Ni2+) / τact(C) - 1], norm.
[Ni2+]o (mol/l)
E
Fractional effect
[Ni2+]o (mol/l)

Fig. 9.

explored voltage range, the $I_{tail}(V)$ plots had a quasi-ohmic, nonrectifying behavior, and could be properly fitted by linear functions. The slope coefficients returned by these linear fittings represent therefore a slope conductance (G_{slope}), and quantify the magnitude of the conductances underlying the currents activated by the strong depolarizing pulses. Figure 10*C* shows the average, percent inhibition exerted by 50-μM Ni^{2+} on G_{slope}. In the same cells, this inhibitory effect of Ni^{2+} was also examined on $P_{Ba}(V)$ plots derived from *I-V* protocols (*see* Fig. 5*A*), as well as from the percent reduction of the maximal amplitude of the "steady-state" component of I_{tail}s (I_{ss} in Fig. 10*A1*). It is apparent from Fig. 10*C* that the inhibitory effect exerted by Ni^{2+} on G_{slope} was moderately, yet significantly lower than that measured on both maximal P_{Ba} and maximal I_{ss} values. These observations indicate that a relatively weak although significant degree of relief from Ni^{2+} block is promoted by strong depolarizations in our experimental system, and are consistent with the idea that Ni^{2+} reduces I_{Ba} amplitude by exerting a true blocking action on the channel pore.

If the partial relief from Ni^{2+} block caused by strong depolarizations actually results from removal of channel-pore obstruction, the deactivation speed of tail currents elicited by repolarization from +60 mV could be expected to be increased, rather than decreased, by Ni^{2+} application, as a consequence of the re-block process. Our data, however, failed to demonstrate such an effect, since the tail currents recorded upon repolarization after steps at +60 mV appeared to be slowed by Ni^{2+} similarly to those evoked after weaker depolarizations (*not shown*). Yet, this observation cannot be considered evidence against a channel-pore blocking mechanism, since the reduction of Ni^{2+}-dependent I_{Ba} inhibition promoted by depolarizations at +60 mV, although consistent and significant, was relatively minor. The effects of a small relief from block could thus be simply masked by an overwhelming slowing effect on channel gating. It should be noted, however, that alternative mechanisms not based on channel-pore block could also account for Ni^{2+}-induced I_{Ba} inhibition and its partial removal by strong depolarizations, including the possibility that Ni^{2+} stabilizes nonconducting channel states in a voltage-dependent manner (*see above*, and Discussion).

Ni^{2+} Artifactually Alters the Voltage Dependence of I_{Ba}s Evoked by Fast Voltage Ramps

The observation that Ni^{2+} is able to modify the gating kinetics of HVA Ca^{2+} currents may have several implications from the experimenter's viewpoint. One of them is the possibility that the Ni^{2+}-dependent decrease of I_{Ba} activation speed may cause alterations in the apparent voltage dependence of I_{Ba}s when ramp, rather than step, voltage protocols are utilized. Indeed, whereas Ni^{2+} caused no significant modification of the voltage dependence of I_{Ba}s activated with depolarizing step protocols (*see above*), the *I-V* relationship of I_{Ba}s elicited with relatively fast (2.6 mV/msec) voltage ramps consistently displayed some degree of rightward shift during application of 50-μM Ni^{2+} (Fig. 11*B1*). The *I-V* relationship of residual, ramp-activated I_{Ba}s was shifted by ~5–10 mV in the positive direction as compared to that of Ni^{2+}-sensitive currents obtained by subtraction (Fig. 11*B2*).

To verify if the latter observation could be explained by the interactions between ramp protocols and the slower I_{Ba} activation kinetics, we performed computer simulations of the effects of Ni^{2+} on ramp-evoked I_{Ba}s. The activation kinetics of I_{Ba}s, both in control conditions and under Ni^{2+}, were modeled on the basis of the experimental data illustrated in Fig. 2*B1*. A single, lumped activation time constant (namely $\bar{\tau}_{act}$: *see above*) was considered for simplicity. The following relation was used for an approximated description of $\bar{\tau}_{act}(V)$ over the voltage range of interest in both control and Ni^{2+} (*see* Fig. 2*B1*):

$$\bar{\tau}_{act} = \tau_A \cdot \exp(-V/V_k) + \tau_C$$

where $V_k = +26.9$ mV, $\tau_A = 1.15$ msec, $\tau_C = 0.05$ msec

Fig. 9. Concentration dependence of the effects of Ni^{2+} on I_{Ba}s. (*A*) I_{Ba}s recorded in a representative neuron (cell C9N16), in response to step depolarizations at various voltage levels (same voltage protocol as shown in Fig. 5*A1*), in control conditions and during application of increasing concentrations of Ni^{2+}. Panel *A1* shows the original current traces, panel *A2* shows the currents recorded at the peak of the *I-V* relationship (0 mV) normalized to their peak amplitudes, superimposed, and expanded in the time scale to highlight their activation phases. Current sampling interval was 50 μsec. The numbers in *A2* are Ni^{2+} concentrations (in μmol/l) relevant to each current trace. (*B*) Average, normalized *I-V* relationships of I_{Ba}s recorded in control conditions (filled circles) and in the presence of increasing concentrations of Ni^{2+} (empty squares, 5 μM; filled triangles, 15 μM; empty diamonds, 50 μM; filled reversed triangles, 150 μM; empty circles, 3 mM). Peak current values have been normalized in each cell to the maximal value, observed at the peak of the *I-V* relationship in control conditions, then averaged among cells, and further normalized to the maximal value of the average, control plot ($n = 10$). (*C*) Average plot of the dependence on extracellular Ni^{2+} concentration ($[Ni^{2+}]_o$) of fractional I_{Ba}-amplitude inhibition $[1 - I_{Ba}(Ni^{2+})/I_{Ba}(C)]$ ($n = 10$). The currents considered for measuring I_{Ba} amplitude were those recorded at the peak of the *I-V* relationship. The smooth line is the best Langmuir fit to data points, with $K_D = 87.8$ μM and $n = 1.088$ (±0.057). (*D*) Average plot of the dependence on $[Ni^{2+}]_o$ of the relative $\bar{\tau}_{act}$ increase under Ni^{2+} *vs.* control conditions $[\bar{\tau}_{act}(Ni^{2+})/\bar{\tau}_{act}(C) - 1]$, normalized in each cell to the maximal value observed ($n = 10$). The currents considered for $\bar{\tau}_{act}$ measurements were those recorded at the peak of the *I-V* relationship. The smooth line is the best Langmuir fit to data points, with $K_D = 185.0$ μM and $n = 1.729$ (±0.323). (*E*) Theoretical functions describing the concentration dependences of both Ni^{2+}-induced fractional I_{Ba} inhibition and relative $\bar{\tau}_{act}$ increase, here shown superimposed for comparison.

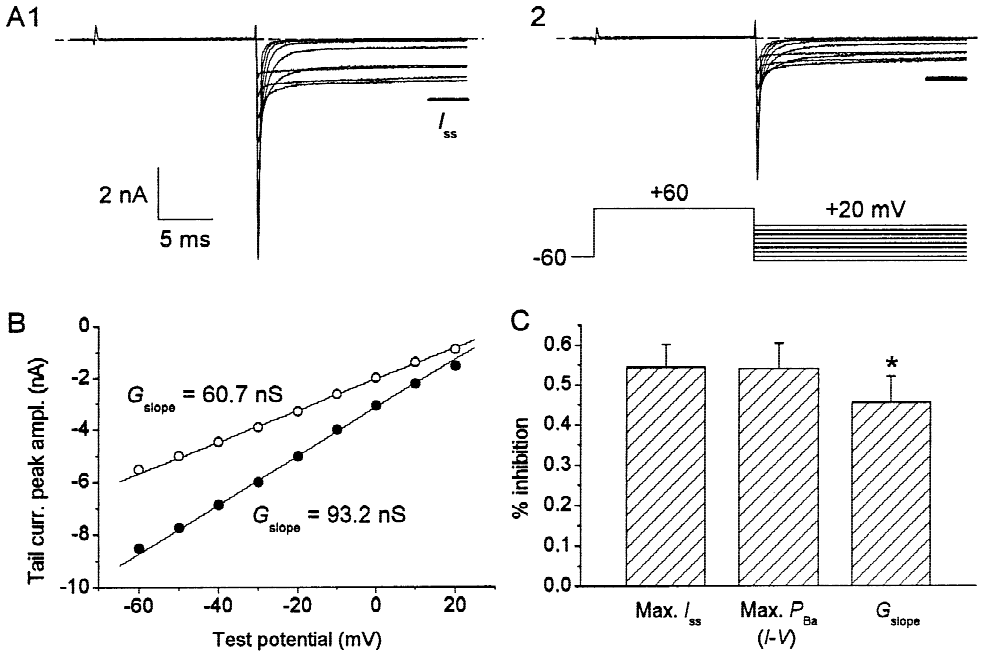

Fig. 10. Strong depolarizing pulses partly and transiently relieve Ni^{2+} block of I_{Ba}s (tail currents). (*A*) Experimental protocol used for testing the effects of strong depolarizations on Ni^{2+}-induced block of I_{Ba}s. Current traces are I_{Ba}s recorded in a representative neuron (cell B0127) in response to the voltage protocol illustrated in the lower part of panel *A2*, in the absence (*A1*) and in the presence (*A2*) of 50-μM Ni^{2+}. Current sampling interval was 20 μsec. The horizontal bars remark the time span over which data points were averaged to obtain a measurement of the maximal amplitude of the "steady-state" current (I_{ss}). (*B*) Plot of the peak amplitude of tail currents elicited by step repolarizations (I_{tail}s) as a function of command voltage. Same cell as illustrated in panel *A*. Straight lines are the best linear fits to data points. The values returned by linear fittings for slope coefficients, which represent macroscopic slope conductances (G_{slope}), are also indicated nearby. (*C*) Average bar diagram of the percent inhibition caused by 50-μM Ni^{2+} on G_{slope}, I_{ss}, and the maximal Ba^{2+} permeability (P_{Ba}) derived from *I-V* protocols (*see* Fig. 5). All of the values were obtained from the same cells ($n = 4$; *, $P < 0.02$ and $P < 0.002$ for the comparison with maximal I_{ss} and P_{Ba}, respectively, according to the *t*-test for paired data).

in control conditions; and $V_k = +23.9$ mV, $\tau_A = 1.89$ msec, $\tau_C = 0.10$ msec in Ni^{2+}.

Numerical reconstructions of I_{Ba}s elicited by 2.6-mV/msec depolarizing voltage ramps were carried out as explained in Materials and Methods. The modeled effects of 50-μM Ni^{2+} on I_{Ba} amplitude and activation kinetics were such that the apparent *I-V* relationship of simulated residual currents was shifted in the positive direction, as compared to that of Ni^{2+}-sensitive currents obtained by subtraction, very similarly to what observed experimentally (Fig. 11*C*). Hence, Ni^{2+}-dependent decrease of I_{Ba} activation speed can artifactually mimic a selective blockade of a low-voltage-activated current component when ramp protocols are used. These findings point to the importance of carefully selecting an appropriate voltage protocol when testing the effects of Ni^{2+} on the biophysical properties of voltage-dependent Ca^{2+} currents.

Discussion

In the present study we show that Ni^{2+} ions affect HVA Ca^{2+} currents expressed by pyramidal neurons from guinea-pig piriform cortex in a dual way. First of all, Ni^{2+} reduces the amplitude of Ba^{2+} currents (I_{Ba}s) with an EC_{50} of about 60 μM. Consistently with a mechanism of channel-pore blockade, already demonstrated in other experimental systems (Chesnoy-Marchais, 1985; Winegar et al., 1991), this effect was partly relieved by strong depolarizations (+60 mV), which are expected to oppose the cation to penetrate the permeation path from the external side of the membrane.

Additionally, we found that nonsaturating concentrations of Ni^{2+} remarkably slowed the activation kinetics of residual HVA currents. "Ni^{2+}-sensitive" currents isolated by subtraction appeared to activate substantially faster than both total and "Ni^{2+}-resistant" currents. We could exclude that this effect was the consequence of a preferential inhibition of some fast-activating current component(s), since none of the components into which the slowly inactivating I_{Ba}s under study can be pharmacologically dissected displayed activation kinetics similar to those of residual or "Ni^{2+}-sensitive" currents. The possibility that the slowing of I_{Ba} activation kinetics resulted from a voltage- and time-dependent relief from Ni^{2+} block upon depolarization could also be ruled out, since: (i) no differences in the percentage of Ni^{2+} block

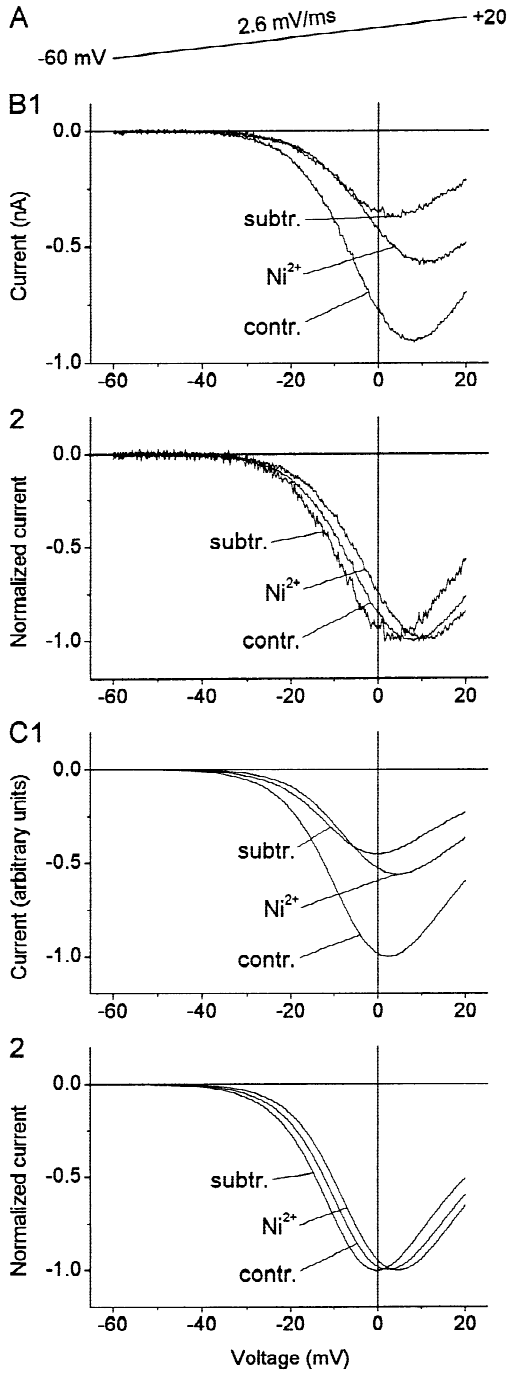

Fig. 11. Ni^{2+} artifactually shifts the *I-V* relationship of Ni^{2+}-insensitive I_{Ba}s in the positive direction in fast voltage-ramp protocols. (*A*) Ramp voltage protocol applied in both real and simulated experiments. (*B*) I_{Ba}s recorded in a representative neuron (cell B9218), in response to the voltage protocol shown in *A*, before and during application of 50-μM Ni^{2+}, and the Ni^{2+}-sensitive current obtained by subtraction. Panel *B1* shows the original, leak-subtracted experimental traces, whereas in panel *B2* the current traces have been normalized to their peak amplitudes. Current sampling interval was 50 μsec. (*C*) Simulated control, Ni^{2+}-insensitive, and Ni^{2+}-sensitive I_{Ba}s returned by the computer modeling of I_{Ba} and of the effects of Ni^{2+} on I_{Ba} amplitude and activation kinetics (*see* text for details). Again, panel *C1* shows the original traces returned by simulation, whereas in panel *C2* the current traces have been normalized to their peak amplitudes.

of the underlying Ba^{2+} permeabilities (P_{Ba}s) were found over the voltage range normally explored for eliciting I_{Ba}s (−30 to +20 mV); (ii) no reduction of Ni^{2+}-induced slowing of I_{Ba}s was observed when depolarizing pulses were delivered from −30 mV (the threshold level for I_{Ba} detection) rather than −60 mV (the usual starting voltage level), thus excluding the existence of a saturating unblocking phenomenon of some current component over the same voltage span.

Our data, therefore, speak out in favor of the only remaining mechanism by which Ni^{2+} could conceivably influence I_{Ba} activation kinetics, namely a direct interference with channel gating processes. In particular, Ni^{2+} would decrease the rate of channel transitions between closed and open states. Such a decrease was primarily demonstrated during I_{Ba} activation, a situation in which the prevalent reaction is that from closed to open state(s). Interestingly, however, our experiments on I_{Ba} deactivation upon repolarization show that the transition rates are also significantly reduced by Ni^{2+} (although to a lesser extent) when the opposite reaction, from open to closed states, is prevalent. As already pointed out in the Results, this observation further confirms that a blocking effect cannot be the only mechanism of action by which Ni^{2+} affects I_{Ba}s in the cells under study. Indeed, the hypothetical existence of a relief from Ni^{2+} block upon depolarization would produce, if anything, an acceleration rather than a slowing of tail currents evoked upon repolarization. Moreover, the decrease of tail-current decay speed caused by Ni^{2+} was found to be even more prominent after prolonged depolarizing test pulses. This observation suggests that time constants are affected more efficiently when deactivation proceeds starting from open states that are favored after long, rather than short, depolarizations. This would introduce the further concept that Ni^{2+} effects also depend on the specific conformational states assumed by the target channels. The idea of a state-dependence of Ni^{2+} effects is in keeping with data already reported by other studies (McFarlane & Gilly, 1998). On the basis of our data on the effects of Ni^{2+} on I_{Ba} activation and deactivation, the following minimal model on the gating of Ca^{2+} channels expressed by our neuronal preparation can be tentatively proposed:

$$C_1 \overset{\tau_1^*}{\leftrightarrow} C_2 \overset{\tau_2^*}{\leftrightarrow} O_1 \overset{\tau_3}{\leftrightarrow} O_2 \overset{\tau_4^*}{\leftrightarrow} C_3 \qquad \text{(Scheme 2)}$$

where the asterisks mark the time constants affected by Ni^{2+}. An intermediate step involving two closed states in the activation pathway (C_1 to C_2) is postulated. Since activation is a much slower process than deactivation, the time constant of the reaction $C_1 \leftrightarrow C_2$ (τ_1) would be

much higher than the time constant that governs the final activation/deactivation step, $C_2 \leftrightarrow O_1$ (τ_2), and rate limiting in the activation process. Moreover, due to the fact that activation time constants are increased by Ni^{2+} much more than deactivation time constants (by ~2.04–2.28 *vs.* ~1.18–1.48 times at −30/−20 mV: *see* Results), τ_1 would be affected by Ni^{2+} significantly more than τ_2. An additional open-to-closed reaction (O_2 to C_3) is also proposed to take into account our observations on the effect of long-lasting depolarizations on deactivation kinetics. Prolonged depolarizations would favor the O_1-to-O_2 transition, and τ_4 (revealed upon repolarization) would be slowed by Ni^{2+} significantly more than τ_2. Of course, a more thorough description of the real situation should keep into account the fact that in our experimental model I_{Ba} activation kinetics were biexponential, which indicates the existence of multiple closed-to-open-state reactions taking place in parallel.

Modifications caused by Ni^{2+} on ionic-channel gating properties have also been reported in other experimental systems. In frog nerve, Ni^{2+} ions slow the activation and inactivation of Na^+ channels (Dodge, 1961; Hille, 1968; Conti et al., 1976). In *Xenopus* oocytes transfected with various Ca^{2+}-channel α_1 subunits, Ni^{2+}, besides blocking HVA Ca^{2+} currents, shifts their voltage dependence of activation in the positive direction (Zamponi, Bourinet & Snutch, 1996). The underlying mechanism has been found to be different from voltage dependence of binding affinity, and has been proposed to consist in an allosteric interaction with the gating machinery. A stabilizing effect of Ni^{2+} on closed, as compared to open, states, which results in a decrease of current activation speed, has been described in a study on a P-type Ca^{2+} current expressed by squid giant fiber lobe neurons (McFarlane & Gilly, 1998). Our data add to those reported in the latter study in several ways: (i) they represent the first demonstration of a Ni^{2+}-induced modification of Ca^{2+}-channel gating in vertebrate neurons; (ii) they show that the effects of Ni^{2+} on I_{Ba} kinetics in mammalian cortical neurons take place at $[Ni^{2+}]_o$ about two orders of magnitude lower than in molluscan neurons, where $[Ni^{2+}]_o$ of 0.3 to 10 mM were necessary; (iii) they provide conclusive evidence that the underlying mechanism does not consist in a voltage- and time-dependent relief from Ni^{2+} block; (iv) they reveal an additional effect of Ni^{2+} that is consistent with a direct Ni^{2+}-dependent modification of channel gating kinetics, but not with a voltage- and time-dependent unblocking process upon depolarization, namely the slowing of deactivation time constants.

Although the results so far discussed rule out the possibility that Ni^{2+}-induced slowing of I_{Ba} activation kinetics depends upon channel-pore block *per se, via* a mechanism of voltage-dependent, slow relief from block upon depolarization, they do not exclude that the same effect may derive from allosteric modifications of channel gating secondary to Ni^{2+} binding to the same channel site whose occupancy results in channel block. However, more light is cast onto this specific issue by another novel finding of ours, namely the observation that the dependence on $[Ni^{2+}]_o$ of the slowing effect on I_{Ba} activation speed was significantly shifted leftwards as compared to that of current-amplitude inhibition. Even more importantly, when the plot of relative $\bar{\tau}_{act}$ *vs.* $[Ni^{2+}]_o$ was fitted with a Langmuir function, the Hill coefficient thus obtained was closer to 2 than 1, in contrast to what observed for the plot describing the concentration dependence of Ni^{2+}-induced I_{Ba} block. This finding strongly suggests that at least one distinct Ni^{2+}-binding site, implicated in the slowing effect on channel gating kinetics, must exist in addition to the one that represents the target of the I_{Ba}-blocking action of Ni^{2+}. Thus, our results from native CNS neurons are in agreement with a previous study on cloned HVA Ca^{2+} channels (Zamponi et al., 1996), in which the existence of additional Ni^{2+}-binding site(s), besides that accounting for channel block, was also proposed, based on a lack of correlation between the effects of Ni^{2+} on channel gating and its blocking action.

The most obvious model that can be proposed to explain the here described effects of Ni^{2+} on voltage-gated Ca^{2+} currents considers, therefore, both interference with channel-state transitions and channel-pore block with Ni^{2+} targeting at least two distinct binding sites. Alternative models could also be imagined. One of these is based on the possibility that Ni^{2+} "stabilizes" Ca^{2+}-channel closed states, or, in other words, that it decreases the rate constants of the closed-to-open reaction more than those governing the opposite process, thereby concomitantly reducing both Ca^{2+}-current amplitude and activation/deactivation speed. This parsimonious hypothesis does not seem to be supported by our finding that the effects of Ni^{2+} on I_{Ba} amplitude and activation kinetics show different dependence on the cation's concentration. Another possibility is that Ni^{2+}, rather than obstructing the Ca^{2+}-channel pore, and besides affecting channel activation kinetics, simply "freezes" a fraction of channels in a nonconducting state. Under the latter hypothesis, Ni^{2+} binding and/or effectiveness should decrease in the presence of channel state(s) favored by strong depolarizations, given our observation that voltage steps at +60 mV partially revert I_{Ba} inhibition. It is also possible that both channel-pore obstruction and stabilization of nonconductive states contribute to the Ni^{2+}-induced inhibitory effect on I_{Ba}. Further investigations will be needed to discriminate the relative importance of these two mechanisms in our experimental system.

In addition to the detailed biophysical characterization of the effects of Ni^{2+} on the Ca^{2+} conductances under study, our data also provide some useful *caveats* to

the experimenter. First of all, the observation that a Ni^{2+}-sensitive current isolated by subtraction displays a faster activation phase than residual current components, and/or a transient phase of fast, partial inactivation (*see* Figs. 1 and 4), should not be automatically interpreted as the indication of intrinsic kinetic differences between conductances characterized by different sensitivity to Ni^{2+}. In our case, such effects were clearly only the artifactual consequence of Ni^{2+}-dependent slowing of residual current activation phase. This indication can be of remarkable importance if we consider that the Ca^{2+}-currents that have been found to be more specifically blocked by Ni^{2+}, namely some T- and R-type currents (*see* Introduction), are also characterized by fast inactivation (*see* Ellinor et al., 1993; Huguenard, 1996; Wang et al., 1997; Scamps et al., 1998). Moreover, the decrease of Ca^{2+}-current activation speed caused by Ni^{2+} can also significantly modify the estimated voltage dependence of the underlying conductance(s) when "instantaneous" *I-V* curves are constructed by delivering fast voltage ramps. We could demonstrate that, in this condition, the voltage dependence of the Ni^{2+}-sensitive current component would be artifactually shifted in the negative direction as compared to that of residual currents, which again may simulate voltage-dependent properties typical of both T- and R-type currents (*see* Huguenard, 1996; Bargas et al., 1994; Tottene, Moretti & Pietrobon, 1996).

In conclusion, our data show that Ni^{2+} can modulate, in a sense, Ca^{2+}-channel function. The question can be raised whether effects similar to those produced by Ni^{2+} on Ca^{2+}-channel kinetics are also carried out by other metal divalent cations of biological importance, e.g., Zn^{2+}, whose roles as a physiological neuromodulator are well known and have been extensively studied (*see* Vallee & Falchuk, 1993). Preliminary data from our laboratory suggest that concentrations of Zn^{2+} within a range of biological relevance can indeed modify Ca^{2+}-current activation kinetics very similarly to what has been described here for Ni^{2+}. This issue, which implies the possible existence of modulatory actions exerted by biologically important divalent cations on Ca^{2+}-channel function, is particularly intriguing and deserves further investigation.

References

Allen, T.G., Sim, J.A., Brown, D.A. 1993. The whole-cell calcium current in acutely dissociated magnocellular cholinergic basal forebrain neurones of the rat. *J. Physiol.* **460:**91–116

Bao, J., Li, J.J., Perl, E.R. 1998. Differences in Ca^{2+} channels governing generation of miniature and evoked excitatory synaptic currents in spinal laminae I and II. *J. Neurosci.* **18:**8740–8750

Bargas, J., Howe, A., Eberwine, J., Cao, Y.., Surmeier, D.J. 1994. Cellular and molecular characterization of Ca^{2+} currents in acutely isolated, adult rat neostriatal neurons. *J. Neurosci.* **14:**6667–6686

Beurrier, C., Congar, P., Bioulac, B., Hammond, C. 1999. Subthalamic nucleus neurons switch from single-spike activity to burst-firing mode. *J. Neurosci.* **19:**599–609

Carbone, E., Swandulla, D. 1989. Neuronal calcium channels: kinetics, blockade and modulation. *Prog. Biophys. Mol. Biol.* **54:**31–58

Chesnoy-Marchais, D. 1991. Kinetic properties and selectivity of calcium-permeable single channels in *Aplysia* neurones. *J. Physiol.* **367:**457–488

Chow, R.H. 1991. Cadmium block of squid calcium currents. Macroscopic data and a kinetic model. *J. Gen. Physiol.* **98:**751–770

Conti, F., Hille, B., Neumcke, B., Nonner, W., Stämpfli, R. 1976. Measurement of the conductance of the sodium channel from current fluctuations at the node of Ranvier. *J. Physiol.* **262:**699–727

Crunelli, V., Lightowler, S., Pollard, C.E. 1989. A T-type Ca^{2+} current underlies low-threshold Ca^{2+} potentials in cells of the cat and rat lateral geniculate nucleus. *J. Physiol.* **413:**543–561

Dodge, F.A. 1961. Ionic permeability changes underlying excitation. *In*: Biophysics of Physiological and Pharmacological Actions. A.M. Shanes, editor. pp. 119–143. American Association for the Advancement of Science, Washington, D.C.

Ellinor, P.T., Zhang, J.-F., Randall, A.D., Zhou, M., Schwartz, T.L., Tsien, R.W., Horne, W.A. 1993. Functional expression of a rapidly inactivating neuronal calcium channel. *Nature* **363:**455–458

Fox, A.P., Nowycky, M.C., Tsien, R.W. 1987. Kinetic and pharmacological properties distinguishing three types of calcium currents in chick sensory neurones. *J. Physiol.* **394:**149–172

Fraser, D.D., MacVicar, B.A. 1991. Low-threshold transient calcium current in rat hippocampal lacunosum-moleculare interneurons: kinetics and modulation by neurotransmitters. *J. Neurosci.* **11:**2812–2820

Gillessen, T., Alzheimer, C. 1997. Amplification of EPSPs by low Ni^{2+}- and amiloride-sensitive Ca^{2+} channels in apical dendrites of rat CA1 pyramidal neurons. *J. Neurophysiol.* **77:**1639–1643

Hille, B. 1968. Charges and potentials at the nerve surface. Divalent ions and pH. *J. Gen. Physiol.* **51:**221–236

Hille, B. 1992. Ionic Channels of Excitable Membranes. Sinauer, Sunderland, MA

Huang, L.Y. 1989. Calcium channels in isolated rat dorsal horn neurones, including labelled spinothalamic trigeminothalamic cells. *J. Physiol.* **411:**161–177

Huguenard, J.R. 1996. Low-threshold calcium currents in central nervous system neurons. *Annu. Rev. Physiol.* **58:**329–348

Kaneda, M., Akaike, N. 1989. The low-threshold Ca current in isolated amygdaloid neurons in the rat. *Brain Res.* **497:**187–190

Lansman, J.B., Hess, P., Tsien, R.W. 1986. Blockade of current through single calcium channels by Cd^{2+}, Mg^{2+}, and Ca^{2+}. Voltage and concentration dependence of calcium entry into the pore. *J. Gen. Physiol.* **88:**321–347

Lee, J.-H., Daud, A.N., Cribbs, L.L., Lacerda, A.E., Pereverzev, A., Klöchner, U., Schneider, T., Perez-Reyes, E. 1999*a*. Cloning and expression of a novel member of the low voltage-activated T-type calcium channel family. *J. Neurosci.* **19:**1912–1921

Lee, J.-H., Gomora, J.C., Cribbs, L.L., Perez-Reyes, E. 1999*b*. Nickel block of three cloned T-type calcium channels: low concentrations selectively block α_{1H}. *Soc. Neurosci. Abstr.* **25:**198

Lucaj, Z., Fujii, J.T. 1994. Multiple subtypes of voltage-gated calcium currents in the Edinger-Westphal nucleus. *Brain Res.* **660:**1–7

Magee, J.C., Carruth, M. 1999. Dendritic voltage-gated ion channels regulate the action potential firing mode of hippocampal CA1 pyramidal neurons. *J. Neurophysiol.* **82:**1895–1901

Magistretti, J., Brevi, S., de Curtis, M. 1999. Biophysical and pharmacological diversity of high-voltage-activated calcium currents in layer-II neurones of guinea-pig piriform cortex. *J. Physiol.* **518:** 705–720

Magistretti, J., Brevi, S., de Curtis, M. 2000. A blocker-resistant, fast-decaying, intermediate-threshold calcium current in paleocortical pyramidal neurones. *Eur. J. Neurosci.* (*in press*)

Magistretti, J., de Curtis, M. 1998. Low-voltage activated T-type calcium currents are differently expressed in superficial and deep layers of guinea pig piriform cortex. *J. Neurophysiol.* **79:**808–816

McFarlane, M.B., Gilly, W.F. 1998. State-dependent nickel block of a high-voltage-activated neuronal calcium channel. *J. Neurophysiol.* **80:**1678–1685

Müller, T.H., Misgeld, U., Swandulla, D. 1992. Ionic currents in cultured rat hypothalamic neurones. *J. Physiol.* **450:**341–362

Ozawa, S., Tsuzuki, K., Iino, M., Ogura, A., Kudo, Y. 1989. Three types of voltage-dependent calcium current in cultured rat hippocampal neurons. *Brain Res.* **495:**329–336

Perez-Reyes, E. 1998. Molecular characterization of a novel family of low voltage-activated, T-type, calcium channels. *J. Bioenerg. Biomembr.* **30:**313–318

Sabatier, N., Richard, P., Dayanithi, G. 1997. L-, N- and T- but neither P- nor Q-type Ca^{2+} channels control vasopressin-induced Ca^{2+} influx in magnocellular vasopressin neurones isolated from the rat supraoptic nucleus. *J. Physiol.* **503:**253–268

Scamps, F., Valentin, S., Dayanithi, G., Valmier, J. 1998. Calcium channel subtypes responsible for voltage-gated intracellular calcium elevations in embryonic rat motoneurons. *Neurosci.* **87:**719–730

Schneider, T., Wei, X., Olcese, R., Costantin, J.L., Neely, A., Palade, P., Perez-Reyes, E., Qin, N., Zhou, J., Crawford, G.D., et al. 1994. Molecular analysis and functional expression of the human type E neuronal Ca^{2+} channel α_1 subunit. *Recept. Chann.* **2:**255–270

Soong, T.W., Stea, A., Hodson, C.D., Dubel, S.J., Vincent, S.R., Snutch, T.P. 1993. Structure and functional expression of a member of the low voltage-activated calcium channel family. *Science* **260:**1133–1136

Swandulla, D., Armstrong, C.M. 1989. Calcium channel block by cadmium in chicken sensory neurons. *Proc. Natl. Acad. Sci. USA* **86:**1736–1740

Takahashi, K., Akaike, N. 1991. Calcium antagonist effects on low-threshold (T-type) calcium current in rat isolated hippocampal CA1 pyramidal neurons. *J. Pharmacol. Exp. Ther.* **256:**169–175

Tottene, A., Moretti, A., Pietrobon, D. 1996. Functional diversity of P-type and R-type calcium channels in rat cerebellar neurons. *J. Neurosci.* **16:**6353–6363

Tottene, A., Volsen, S., Pietrobon, D. 2000. α_{1E} subunits form the pore of three cerebellar R-type calcium channels with different pharmacological and permeation properties. *J. Neurosci.* **20:**171–178

Vallee, B.L., Falchuk, K.H. 1993. The biochemical basis of zinc physiology. *Physiol. Rev.* **73:**79–118

Wakamori, M., Niidome, T., Furutama, D., Furuichi, T., Mikoshiba, K., Fujita, Y., Tanaka, I., Katayama, K., Yatani, A., Schwartz, A., Mori, Y. 1994. Distinctive functional properties of the neuronal BII (class E) calcium channel. *Recept. Chann.* **2:**303–314

Wang, G., Dayanithi, G., Kim, S., Hom, D., Nadasdi, L., Kristipati, R., Ramachandran, J., Stuenkel, E.L., Nordmann, J.J., Newcomb, R., Lemos, J.R. 1997. Role of Q-type Ca^{2+} channels in vasopressin secretion from neurohypophysial terminals of the rat. *J. Physiol.* **502:**351–363

Wang, Y., Rowan, M.J., Anwyl, R. 1997. LTP induction dependent on activation of Ni^{2+}-sensitive voltage-gated calcium channels, but not NMDA receptors, in the rat dentate gyrus in vitro. *J. Neurophysiol.* **78:**2574–2581

Williams, M.E., Marubio, L.M., Deal, C.R., Hans, M., Brust, P.F., Philipson, L.H., Miller, R.J., Johnson, E.C., Harpold, M.M., Ellis, S.B. 1994. Structure and functional characterization of neuronal α_{1E} calcium channel subtypes. *J. Biol. Chem.* **269:**22347–22357

Winegar, B.D., Kelly, R., Lansman, J.B. 1991. Block of current through single calcium channels by Fe, Co, and Ni. Location of the transition metal binding site in the pore. *J. Gen. Physiol.* **97:**351–367

Yang, J., Ellinor, P.T., Sather, W.A., Zhang, J.-F., Tsien, R.W. 1993. Molecular determinants of Ca^{2+} selectivity and ion permeation in L-type Ca^{2+} channels. *Nature* **366:**158–161

Ye, J.H., Akaike, N. 1993. Calcium currents in pyramidal neurons acutely dissociated from the rat frontal cortex: a study by the nystatin perforated patch technique. *Brain Res.* **606:**111–117

Zamponi, G.W., Bourinet, E., Snutch, T.P. 1996. Nickel block of a family of neuronal calcium channels: subtype- and subunit-dependent action at multiple sites. *J. Membrane Biol.* **151:**77–90

Zhang, J.F., Randall, A.D., Ellinor, P.T., Horne, W.A., Sather, W.A., Tanabe, T., Schwarz, T.L., Tsien, R.W. 1993. Distinctive pharmacology and kinetics of cloned neuronal Ca^{2+} channels and their possible counterparts in mammalian CNS neurons. *Neuropharmacol.* **32:**1075–1088